Modeling by disruption and a selected-for partner for the nude locus

Jian Li[1,2,†] , Yun-Kyoung Lee[1,†] , Wenyu Fu[1,2], Anne M Whalen[2], Mario C Estable[3], Laurel A Raftery[2,‡] , Kristin White[2] , Lorin Weiner[1,2,*] & Janice L Brissette[1,2,**]

Abstract

A long-standing problem in biology is how to dissect traits for which no tractable model exists. Here, we screen for genes like the nude locus (*Foxn1*)—genes central to mammalian hair and thymus development—using animals that never evolved hair, thymi, or *Foxn1*. Fruit flies are morphologically disrupted by the FOXN1 transcription factor and rescued by weak reductions in fly gene function, revealing molecules that potently synergize with FOXN1 to effect dramatic, chaotic change. Strong synergy/effectivity in flies is expected to reflect strong selection/functionality (purpose) in mammals; the more disruptive a molecular interaction is in alien contexts (flies), the more beneficial it will be in its natural, formative contexts (mammals). The approach identifies *Aff4* as the first nude-like locus, as murine AFF4 and FOXN1 cooperatively induce similar cutaneous/thymic phenotypes, similar gene expression programs, and the same step of transcription, pre-initiation complex formation. These AFF4 functions are unexpected, as AFF4 also serves as a scaffold in common transcriptional-elongation complexes. Most likely, the approach works because an interaction's power to disrupt is the inevitable consequence of its selected-for power to benefit.

Introduction

Many human traits evolved long before humans did and have been conserved to the present day in easily manipulated, genetically dissectible organisms, allowing these organisms to serve as tractable scientific models. Collectively, these models have generated much of what is known about the living world, as countless shared traits and biological principles have been elucidated through their use. Still, every trait is not widely shared: Novelties have appeared in every branch of the evolutionary tree, often in series with innovation building on innovation, and with phenotypic novelties arising in part from genetic novelties. As such, many traits are not tractably modeled, as easily manipulated forms of life never evolved the relevant novelties, and pliable *in vitro* systems have not reproduced the traits. Overall, this lack of models is among the most long-standing problems in the biological sciences: One way or another, it obstructs the elucidation of every trait specific to organisms unsuited for genetic dissection. As the problem stems from the immutable reality of evolutionary history, a complete solution may never be found. Nonetheless, there should be ways to lessen the problem and model more traits. For example, while model organisms may lack a specific trait, they often possess some, if not all, of the trait's building blocks, i.e., ancient molecules or segments of molecules that were reorganized by evolution and progressively assembled into a novelty (reviewed in Graur & Li, 2000). In certain circumstances, these libraries of building blocks might be drawn on so as to recreate units of function (modules) within novelties, thereby revealing genes important for those functions.

In the study described here, we sought to identify genes with a uniquely mammalian function, namely a function like that of the nude locus, which regulates aspects of mammalian development and was first revealed by the nude mouse. The nude mouse was discovered ~54 years ago, and since then, its odd mix of abnormalities has made it one of the best known and highly used mutant animals (for reviews of the nude phenotype, see Mecklenburg *et al*, 2005; Weiner *et al*, 2014; Vaidya *et al*, 2016; Rota & Dhalla, 2017). Its signature and most striking abnormalities are the lack of a thymus and hair coat, two outwardly unrelated traits whose absence makes nude animals particularly well suited for the grafting and observation of foreign cells. Other defects of nude mice include the abnormal keratinization of the epidermis, the loss of pigment-recipient cells, and the aberrant differentiation of nails. Nude phenotypes

1   Department of Cell Biology, State University of New York Downstate Health Sciences University, Brooklyn, NY, USA
2   Cutaneous Biology Research Center, Massachusetts General Hospital and Harvard Medical School, Charlestown, MA, USA
3   Department of Chemistry and Biology, Ryerson University, Toronto, ON, Canada
    *Corresponding author. Tel: +1 718 270 3778; E-mail: lorin.weiner@downstate.edu
    **Corresponding author. Tel: +1 718 270 3755; E-mail: janice.brissette@downstate.edu
    †These authors contributed equally to this work
    ‡Present address: School of Life Sciences, University of Nevada Las Vegas, Las Vegas, NV, USA

were subsequently identified in rats, cats, and humans, with the human condition known clinically as T-cell immunodeficiency, congenital alopecia, and nail dystrophy. The nude phenotype thus signals the existence of a core developmental mechanism shared by the mammalian skin and thymus.

To date, the nude phenotype has only one known cause and that is the inactivation of FOXN1 (WHN, HFH11), the product of the nude locus and a protein well conserved among mammals (86% identical in mice and humans) (Abitbol *et al*, 2015; Frank *et al*, 1999; Nehls *et al*, 1994; Segre *et al*, 1995; see also Mecklenburg *et al*, 2005; Rota & Dhalla, 2017). FOXN1 is thought to function primarily as a transcriptional activator, as it binds to DNA with sequence specificity via a forkhead domain (Schlake *et al*, 1997) and upregulates a variety of gene transcripts or reporter constructs, directly in some cases, perhaps indirectly in others (Brissette *et al*, 1996; Schüddekopf *et al*, 1996; Schlake *et al*, 1997; Schlake *et al*, 2000; Schorpp *et al*, 2000; Mecklenburg *et al*, 2005; Weiner *et al*, 2007; Mandinova *et al*, 2009; Nowell *et al*, 2011; Bredenkamp *et al*, 2014b; Vaidya *et al*, 2016; Zuklys *et al*, 2016; and references therein). Nonetheless, much remains unknown about FOXN1, in particular, its mechanism of gene upregulation, its key sets of targets/effectors, and the larger regulatory system to which it belongs.

As 54 years have passed without the discovery of a second nude locus, FOXN1 clearly performs an unusual function and may be unique in the precise combination or impact of its actions. Nonetheless, as *Foxn1* surely does not act alone, we expected other genes to perform functions like those of *Foxn1* and hence to constitute nude-like loci—loci that produce cutaneous and thymic phenotypes resembling those of *Foxn1*. To find these nude-like loci, the direct approach would be to use forward genetics, i.e., to screen mutagenized mice for nude-like phenotypes and then to identify the responsible mutated genes. Forward genetics is widely recognized as a uniquely powerful approach, as it directly reveals genes of a specified significance to a living system, typically the genes that generate a trait of interest. Given the practical difficulty of screening mammals however, we sought to perform forward genetics with a tractable stand-in for the mouse.

We chose the fruit fly *Drosophila melanogaster* due to its molecular homologies with mammals and ease of genetic manipulation. This animal was not a natural model for our traits of interest, however. At the phenotypic level, flies lack hair and thymi, the traits most affected by nude mutations. In fact, flies lack skin and lymphocyte-based adaptive immune systems, the broader traits to which hair and thymi belong. While fly bristles superficially resemble hair, these cylindrical projections are not related to hair and instead are homologous to microvilli and stereocilia (Tilney & DeRosier, 2005), with their rigidity provided by chitin-based exoskeletons.

Furthermore, at the molecular level, flies lack a clear equivalent to FOXN1, the central player in the nude phenotype. The fly protein most similar to FOXN1 is Jumu (Dom, Dwhn), a transcription factor with a forkhead DNA-binding domain that is similar in sequence to FOXN1's forkhead domain (Cheah *et al*, 2000; Strodicke *et al*, 2000; Sugimura *et al*, 2000). However, FOXN1 and Jumu possess little if any similarity outside their short DNA-binding domains—the two proteins differ in 86% or more of their overall sequence. Additionally, FOXN1 and Jumu appear to have different DNA-binding specificities, GACGC in the case of FOXN1 (Schlake *et al*, 1997; Zuklys *et al*, 2016) versus CACC (Sugimura *et al*, 2000), ACAACA (Zhu *et al*,

2012), or methylated adenine residues (He *et al*, 2019) in the case of Jumu. Hence, the forkhead domains of FOXN1 and Jumu appear to differ in actual function, despite the amino acid similarity. Moreover, the regulation and physiological role of Jumu have no clear correspondence to that of FOXN1, as Jumu appears to be present in early embryos ubiquitously and in many tissues thereafter, generates lethal pleiotropic effects when mutated, and functions as a transcriptional repressor or inducer of heterochromatin formation in at least some situations (He *et al*, 2019; Cheah *et al*, 2000; Strodicke *et al*, 2000; Sugimura *et al*, 2000). Lastly, FOXN1 appears unable to substitute for Jumu in flies, as the abnormalities of *jumu* loss-of-function mutants were not rescued by FOXN1 (introduced via a transgene) but were rescued by Jumu (using the same methodology) (Hofmann *et al*, 2010; our unpublished data). Thus, the differences between FOXN1 and Jumu appear greater than the similarities. These differences presumably made FOXN1 a failed stand-in for Jumu and conversely make Jumu a flawed stand-in for FOXN1.

As FOXN1 is not clearly present in flies but is central to our mechanism of interest in the skin and thymus, we modified flies so as to model FOXN1 function specifically and thereby identify other genes central to the cutaneous/thymic mechanism. The results suggest a simple route to elucidating novel mechanisms when the mechanisms belong to organisms unsuited to standard genetics.

Results

Rationale and outline for a FOXN1 suppressor screen

Cross-species fly models—in particular, flies that produce human gene products from transgenes—have been used successfully in various contexts, most notably, to reproduce and analyze known gene functions (e.g., functions in cell division; de Nooij & Hariharan, 1995), to assay for and analyze novel gene functions (e.g., functions in cell growth; Xu *et al*, 2008), or to replicate diseases caused by the gene products and then screen for genetic modifiers (e.g., neurological disease modifiers; reviewed in McGurk *et al*, 2015). Critically, these human gene products affected fly physiology in ways that were obviously like or related to their effects on human physiology. The fly models thus possessed a validating resemblance to the human traits of interest, typically cellular traits, and this correspondence in fly and human phenotypes proved the models' relevance.

Accordingly, we produced FOXN1 in flies from transgenes. However, these FOXN1 transgenics were unlikely to show any obvious similarity to a known FOXN1 phenotype or activity. The mammalian phenotypes dependent on FOXN1 (e.g., hair coat, thymus) require intricate developmental programs not present in flies. And flies have no processes that FOXN1 would be expected to regulate, as flies seemingly have no FOXN1 and thus have no traits or genes that FOXN1 would necessarily control. Unlike traditional model systems therefore, a FOXN1 fly model could not be based on an obvious likeness to the traits being modeled.

Nonetheless, in flies, FOXN1 was likely to find DNA-binding sites (GACGC) and other molecules important for its function in mammals—e.g., individual proteins, multimolecular complexes, multicomplex modules, or entire pathways—as many aspects of gene regulation, cell physiology, and tissue development are

conserved across animal phyla. Accordingly, we expected FOXN1 to engage this molecular library so as to generate selected-for interactions—interactions that in their natural context (mammals in this case) perform influential functions, yield advantageous traits, and accordingly were selected for during evolution. We expected selected-for interactions to be favored and often powerful, as FOXN1 was presumably shaped by selection to engage in these interactions preferentially, and selection acted upon these interactions precisely because they have "effectivity"; i.e., they make things happen, things that effect phenotypes and thereby affect survival or reproduction. As these interactions would be ectopic, they presumably would be disruptive and visibly so if potent enough. Hence, we sought for FOXN1 to create simply an obvious disruption.

At the same time, we expected FOXN1 to engage directly or indirectly in many interactions that were purposeless or artefactual, as in its alien context and transgene-driven quantities, FOXN1 would surely affect molecules that it would not normally affect and induce responses or outcomes that it would not normally induce. To separate selected-for interactions from purposeless/artefactual ones, we carried out a genetic screen with 3 key elements. Firstly, the fly genome was screened for suppressors of FOXN1 phenotypes, i.e., mutations that rendered FOXN1 visibly impotent and restored fly traits to normal. Secondly, once isolated, FOXN1 suppressors were tested for FOXN1 specificity, that is, a failure to suppress other transgenic phenotypes, which were generated using the same transgenic promoters but different proteins. This test separated suppressors of FOXN1 from suppressors of the transgenic promoters or protein toxicity in general. Thirdly, the screen was conducted with hemizygous deletions, deletions present on one member of a chromosomal pair but not the other. Typically, such deletions are weak loss-of-function mutations, as they leave most (50% or more) of a gene pair's function intact and accordingly have weak effects or no effect at all on phenotypes.

Hemizygous deletions were expected to facilitate both the screening process itself and the identification of genes with a particular significance. In our fly model, if weakly reducing a gene's function restores fly phenotypes to normal, then FOXN1 and the gene product must act with strong synergy, as a small decrease in the activity of one molecule leads to a large decrease in the output or consequences of two molecules. Moreover, if reducing this synergistic interaction prevents an abnormal phenotype from developing, then the interaction must possess a primacy in the event chain leading to the phenotype, making the interaction a root cause of the phenotype and a high-impact catalyst of changes in fitness. We predicted that this combination of synergy and effectivity was likely to characterize selected-for interactions: that is, the isolated molecules interacted with FOXN1 in this powerful way because FOXN1 evolved to interact with them and thereby perform its beneficial function in mammals. This prediction was subsequently tested in mice.

A fly model for FOXN1 function

FOXN1 transgenic flies were generated using the GAL4/UAS system, a bigenic expression system in which one transgene (the target gene) produces the gene product of interest and the second transgene (the driver) produces a transcription factor, GAL4, needed to activate the target gene (Brand & Perrimon, 1993). Our target gene construct, *UAS-Foxn1*, expressed the complete coding sequence of

wild-type murine FOXN1 and in the absence of a driver did not yield any obvious abnormalities.

To generate flies for the suppressor screen, we tested the effects of *UAS-Foxn1* with two different drivers: *GMR-GAL4* (Freeman, 1996) and *hs-GAL4* (Brand *et al*, 1994). *GMR-GAL4* drives target gene expression specifically in the developing eye and hence was used to target FOXN1 to an organ that is easily observed, molecularly complex, and nonessential for viability in the laboratory. *hs-GAL4* drives target gene expression throughout the fly at levels that increase with temperature and thus was used to place FOXN1 in the broadest possible cellular contexts.

When activated by *GMR-GAL4*, *UAS-Foxn1* induced a rough-eye phenotype, as the eye lost its finely latticed structure and instead appeared disorganized, bumpy, and cratered (Fig 1A and B). Rough eyes are the aggregate consequence of disrupted ommatidia ("unit eyes") and are known to result from many types of molecular/cellular abnormalities. A rough-eye phenotype was visible in virtually all *GMR-GAL4/UAS-Foxn1* transgenics and was accompanied by variable defects in ocular pigmentation and interommatidial bristles. The FOXN1 protein was detected in the heads of *GMR-GAL4/UAS-Foxn1* adults by immunoblotting (unpublished observation), suggesting that FOXN1 drove the ommatidial disruption.

When activated by *hs-GAL4*, *UAS-Foxn1* produced two phenotypes: (i) a lethal phenotype in which adults died within 18 h of emergence from the pupal case, and death rates increased from 25% (58/228) to 74% (169/228) to 93% (553/593) as the cultivation temperature increased from 18°C to 25°C to 29°C; and (ii) a white-bristle phenotype in which rising temperatures led to dorsal bristles losing their black pigmentation and becoming misshapen (Fig 1C and D), consistent with the need for pigment in the hardening of the exoskeleton. Similar lethal/white-bristle phenotypes were observed in a previous study of FOXN1's effects in flies (Hofmann *et al*, 2010). None of the FOXN1 transgenic phenotypes (rough eye, lethal, or white bristle) resulted from an evident mimicry (gain) of Jumu function, as four different loss-of-function mutations in *jumu* —*jumu^{Hp126}*, *jumu^{X3}*, *jumu^{D631}*, and *jumu^{2.12}* (Strodicke *et al*, 2000; Sugimura *et al*, 2000)—failed to suppress the abnormalities of the *GMR-GAL4/UAS-Foxn1* or *hs-GAL4/UAS-Foxn1* flies (not shown). Thus, *UAS-Foxn1* powerfully disrupted fly traits when expressed specifically in the eye or more broadly with heat.

A suppressor of FOXN1 phenotypes

We chose to screen for suppressors of the rough-eye phenotype, as this phenotype seemed more likely to be rescued by a single hemizygous deletion than the lethal phenotype (which potentially resulted from multi-organ failure and multiple causes) and seemed likely to yield a broader range of suppressors than the white-bristle phenotype. As the source of hemizygous deletions, we used the Bloomington Deficiency Kit, a collection of fly strains carrying large, defined chromosomal deletions (deficiencies; *Df*) that cover most of the genome and facilitate efficient screening, as *D. melanogaster* possesses nearly as many protein-coding genes as humans (~14,000 in *D. melanogaster* versus ~20,000 in humans; see the NCBI Gene Statistics or CCDS databases) but packs these genes into a genome that is ~1/20th the size and divided into just 4 pairs of chromosomes. During the primary screen, each deletion was assayed individually for dominant suppression of the rough-eye phenotype of
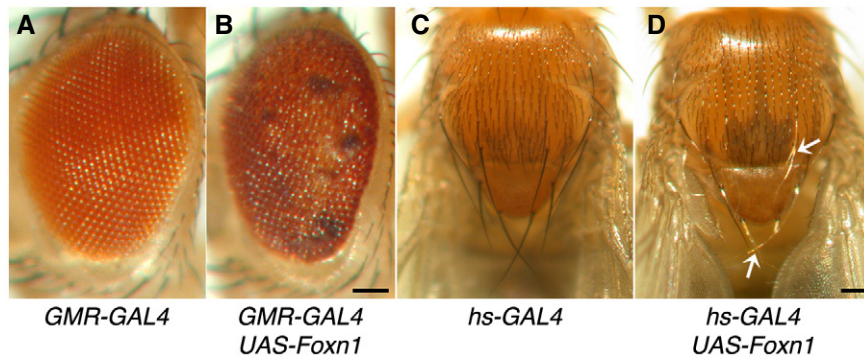
Figure 1. FOXN1 disrupts eye and bristle development in flies.

A, B   Flies form well-organized compound eyes when they carry *GMR-GAL4* without a target gene (A) but develop rough eyes when *GMR-GAL4* drives expression of *UAS-Foxn1* (B).

C, D   Bristles are pigmented and properly shaped when flies carry *hs-GAL4* without a target gene (C) but are often white, bent, and shortened when *hs-GAL4* drives expression of *UAS-Foxn1* (D). Flies in panels (C, D) were raised at 25°C. Arrows denote examples of white bristles.

Data information: Representative phenotypes are shown in all panels. Scale bars, 100 μm.

GMR-GAL4 UAS-Foxn1 flies. Each isolated suppressor was then tested for effects on the rough-eye phenotype generated by *GMR-p21* (de Nooij & Hariharan, 1995), a transgene that employs the same promoter as *GMR-GAL4* but produces human p21 (CDKN1A), a protein with no known relationship to FOXN1. Any mutation that suppressed the FOXN1 and p21 eye phenotypes was considered to lack FOXN1 specificity and was excluded from further study.

The primary screen identified 4 FOXN1 suppressors that were not p21 suppressors. These "FOXN1-specific" suppressors were associated with the following 4 non-overlapping deletions (putative deleted segments appear in parentheses): (i) *Df(1)v-N48* (X chromosome, cytological region 9F to 10C5), (ii) *Df(2L)23C;23E3-6* (chromosome 2, 23C to 23E3-6), (iii) *Df(2L)E110* (chromosome 2, 25F3 to 26D11), and (iv) *Df(3L)fz-M21* (chromosome 3, 70D2 to 71E5). To focus our effort, we initiated mapping experiments for two of these suppressors (the two on chromosome 2), and the first suppressor to be identified was located within *Df(2L)23C;23E3-6*. This gene was *lilli* (lilliputian), the product of which is a likely transcriptional regulator and essential in flies (Tang *et al*, 2001; Wittwer *et al*, 2001). *lilli* then became the focus of our studies.

When flies carried one wild-type *lilli* allele (*lilli*[+]) and one *lilli* allele disrupted by P-element insertion, the FOXN1 rough-eye phenotype was suppressed, as the ommatidia were restored to a near normal pattern and morphology (Fig 2). This genetic suppression was obtained with two different P-element insertion alleles, *lilli*[00632] (Tang *et al*, 2001) and *lilli*[k05431] (Wittwer *et al*, 2001), both of which are ordinarily recessive to *lilli*[+] and hence likely to yield a weak reduction in Lilli function when heterozygous with *lilli*[+]. The rescue of eye phenotypes by *lilli* insertion mutations was even more striking if FOXN1 was produced via a different eye-specific driver, *ey-GAL4* (Hazelett *et al*, 1998), which is active at an earlier stage of eye development than *GMR-GAL4*. *ey-GAL4 UAS-Foxn1* flies lost ommatidia and exhibited a small-eye phenotype when their genetic background was *lilli*^{+/+} (Fig EV1); when one *lilli* insertion allele was introduced, creating *lilli*[+/00632] (Fig 2) or *lilli*[+/k05431] (not shown), the ommatidia were regained, and the eyes were restored to a condition close to wild-type.

To confirm the specificity of *lilli*'s effects on FOXN1, we examined whether the *lilli* insertion mutations dominantly suppressed the rough-eye phenotypes of 3 other transgenics: (i) *GMR-p21*, (ii) *GMR-GAL4 UAS-Med*, in which the target gene expressed *Medea* (Sutherland *et al*, 2003), the *Drosophila* homolog of *Smad4*, or (iii) *ey-GAL4 UAS-Med*. In all 3 cases, the rough-eye phenotypes were not suppressed by the *lilli* mutations, suggesting that *lilli* has a specific interaction with FOXN1 and that this interaction is more potent than any effect *lilli* may have on driver expression (Tang *et al*, 2001), GAL4, or toxic proteins in general. Outside the eye, the *lilli* insertion mutations dominantly suppressed the white-bristle phenotype of the *hs-GAL4 UAS-Foxn1* flies, as the frequency of flies with normal bristle pigmentation increased over 10-fold when the number of *lilli*[+] alleles was cut in half (Fig 2). The *lilli* mutations did not suppress the lethal phenotype of *hs-GAL4 UAS-Foxn1* flies, consistent with the lower probability of rescuing this phenotype with a single weak mutation but also consistent with driver/target gene expression remaining strong in the presence of *lilli* mutations. In sum, weak reductions in *lilli* function rendered FOXN1 largely impotent in the eye and other locations. Wild-type *lilli* thus greatly amplified FOXN1's output and enabled FOXN1 to make a substantial impact on animal phenotypes and fitness. In short, the interaction between *lilli* and FOXN1 exhibited synergy and effectivity.

FOXN1 and the mammalian homologs of Lilli

lilli is homologous to four genes found in humans and other mammals, which are known collectively as the *AF4/FMR2* family (*AFF*) and individually as *AFF1* (*AF4, MLLT2*), *AFF2* (*FMR2*), *AFF3* (*LAF4*), and *AFF4* (*MCEF, AF5Q31*). The similarity of each AFF to Lilli is located in a "Lilli-like segment", which spans the C-terminal two-thirds of each AFF and contains three domains shared with Lilli (Fig 3A) (reviewed in Gu & Nelson, 2003). Notably, chromosomal translocations that fuse the Lilli-like segment of an AFF to the N-terminus of MLL, creating MLL-AFF fusion proteins, are frequently observed drivers of acute leukemias, suggesting that the Lilli-like segment has a potent autonomous function. The full-length AFFs
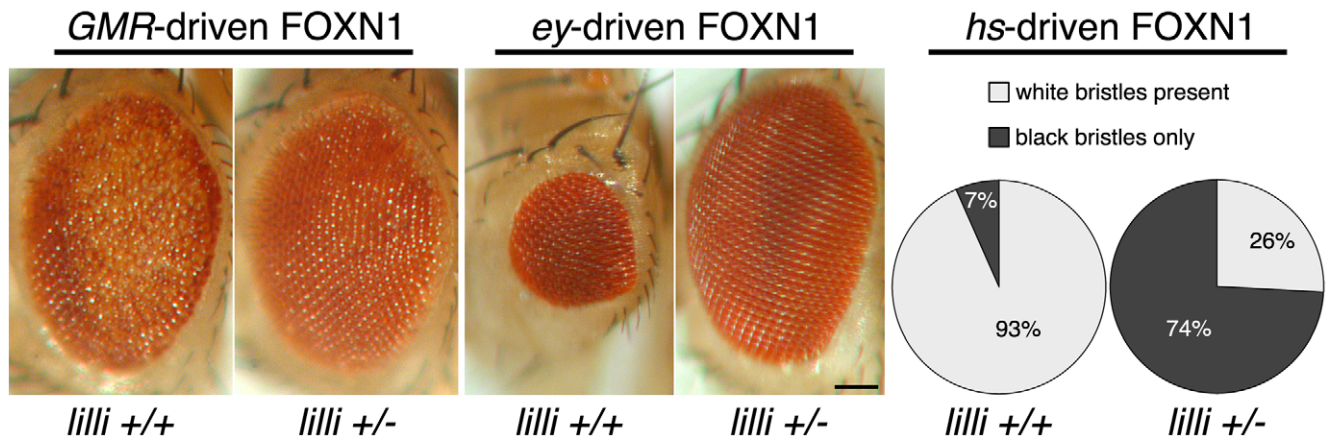
Figure 2. FOXN1 loses disruptive power when *lilli* function is weakly reduced.

In flies with two wild-type *lilli* alleles (*lilli +/+*), *UAS-Foxn1* activity generates rough-eye (*GMR-GAL4*), small-eye (*ey-GAL4*), or white-bristle (*hs-GAL4*) phenotypes, depending on the GAL4 driver used. These morphological disruptions were prevented when the loss-of-function allele *lilli*[00632] was introduced and the number of wild-type *lilli* alleles was reduced to one (*lilli +/-*). Pie charts indicate the percentage of flies in which white bristles were present or completely absent (black bristles only); a total of 212 *lilli +/+* and 232 *lilli +/-* flies were scored, after being raised at 25°C. Scale bar, 100 μm.

are transcription factors and, along with MLL-AFF fusion proteins, are thought to facilitate the elongation phase of transcription (see Discussion).

To assess potential *Aff/Foxn1* interactions, *Aff* gene expression was compared to that of *Foxn1*, which is normally expressed in specific epithelial cell populations of the skin and thymus. As judged by *in situ* hybridization and immunostaining, *Aff1, Aff2,* and *Aff3* were not co-expressed with *Foxn1* in cutaneous or thymic cells (unpublished results), suggesting a lack of any direct interaction between *Foxn1* and these *Aff*s.

In contrast, the expression pattern of *Aff4* conspicuously overlapped with that of *Foxn1*. AFF4 and FOXN1 were present together in the nuclei of epithelial cells in the differentiating cortex of the hair shaft, the differentiating layers of the epidermis (murine or human), and the cortex and medulla of the thymus (Figs 3B–E and EV2). As such, virtually every cell that possessed FOXN1 also possessed AFF4. Conversely, AFF4 had a broader distribution than FOXN1, as AFF4 appeared in more cells in the skin and thymus. Nonetheless, most if not all AFF4-positive cells in the thymus appeared to be epithelial cells and hence were most likely derived from FOXN1-positive cells, as FOXN1-positive cells give rise to most if not all of the thymic epithelium, and this epithelium fails to grow beyond a limited pool of progenitors when FOXN1 is absent (nude mutants) (reviewed in Vaidya *et al*, 2016). In the skin, AFF4 appeared most abundant in the differentiating epithelial cells of the hair cortex. The differentiating hair cortex is also the cutaneous site where FOXN1 appears most abundant and where development is most impaired in nude mutants. Thus, AFF4 is particularly prominent in the cell populations where FOXN1 plays its most important roles. This prominent co-localization suggested that AFF4 might interact with FOXN1 as *lilli* did and so synergize with FOXN1 to effect strong phenotypic change.

Generation of novel *Aff4* alleles

Aff4 has been mutated in mice (Urano *et al*, 2005), but the effects of this germline mutant allele, *Aff4⁻*, were variable and difficult to

interpret. Most *Aff4⁻* homozygotes died during gestation or shortly after birth for unclear reasons, but a minority survived to adulthood and appeared normal, except for a defect in late-stage spermatogenesis, resulting in male sterility. Notably, the *Aff4⁻* mutation deletes the N-terminus of AFF4 but leaves the coding sequence of the entire Lilli-like segment intact.

As the Lilli-like segment was likely to be the critical mediator of any interaction between AFF4 and FOXN1, we generated a murine *Aff4* allele, *Aff4flox*, in which the entire Lilli-like segment could be ablated conditionally. *loxP* sites were inserted at positions flanking exons 10 and 11, which encode amino acids 404–764 of the 1,160 a.a. AFF4 protein (Figs 4A and EV3). As such, Cre-mediated *loxP* recombination would delete 31% of the coding sequence and introduce a frameshift mutation, which in turn would ablate the remaining 34% of AFF4 downstream (Fig 4A). The resulting knockout allele, *Aff4ko*, should accordingly lack all *lilli*-like function and most likely lack all *Aff4* function, as 65% of AFF4 would be replaced by an essentially arbitrary sequence of amino acids.

Two independent *Aff4flox* murine lines were generated, confirmed by Southern blotting (Fig EV3), used in all subsequent studies, and found to yield identical results. *Aff4flox/flox* homozygotes appeared identical to wild-type mice, suggesting that *Aff4flox* is equivalent to wild-type *Aff4* (*Aff4⁺*).

AFF4 and the morphogenesis of the skin

To generate a cutaneous loss of AFF4 function, we utilized the transgene *KRT14-cre* (Li *et al*, 2001), which is active in epithelial stem/progenitor cells of the epidermis and hair follicles and hence should ablate AFF4 throughout the cutaneous epithelium before FOXN1 becomes active. When *KRT14-cre* was crossed onto an *Aff4⁺/flox* background, the *Aff4ko* allele was easily detected by PCR of tail DNA, and no abnormalities were observed, suggesting that *Aff4ko* is recessive to *Aff4⁺*.

When *KRT14-cre; Aff4flox/flox* mice were generated, the result was a hair phenotype with a resemblance to the nude phenotype. Like
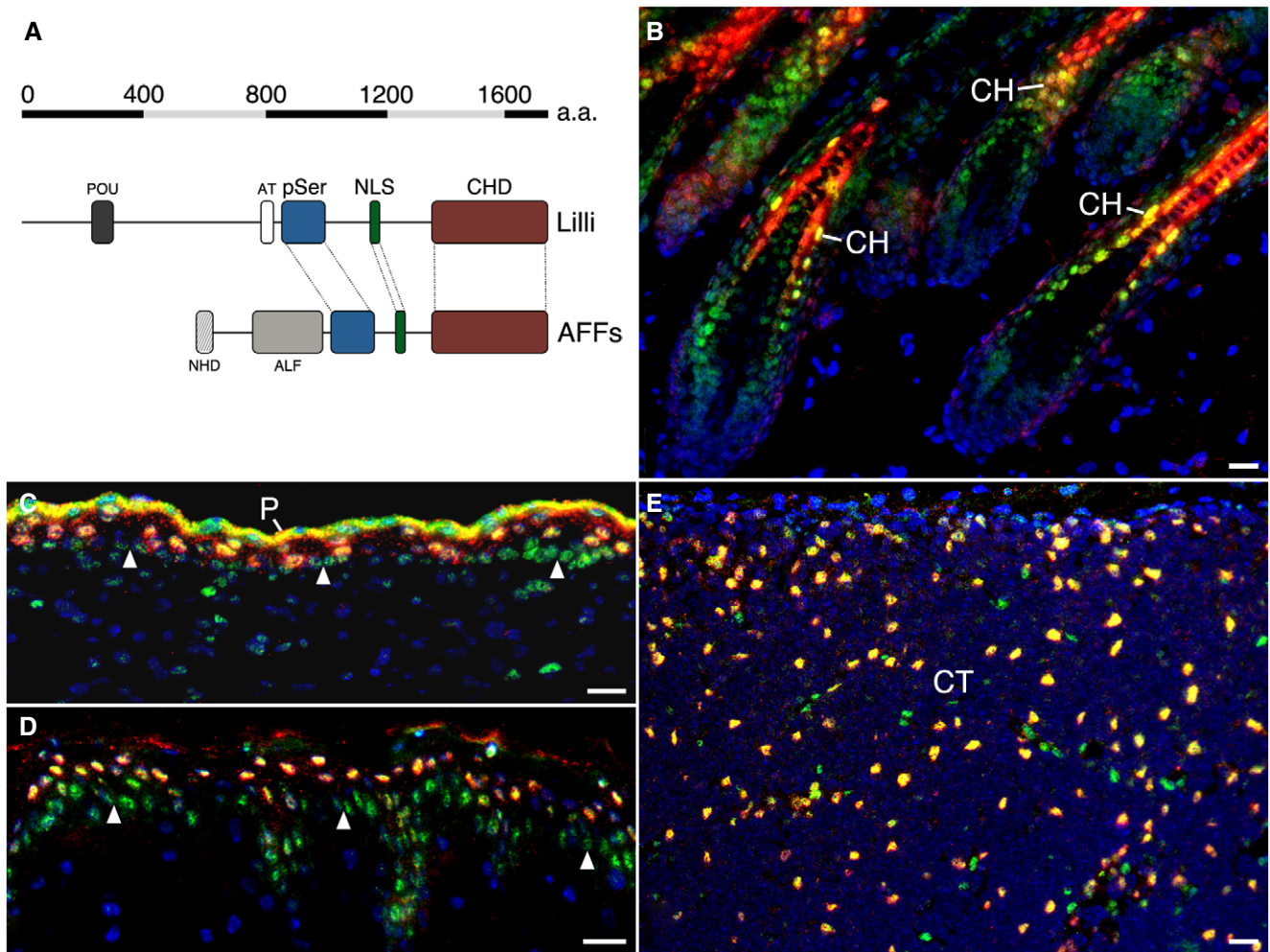
Figure 3. The Lilli homolog AFF4 is positioned to interact with FOXN1 in the skin and thymus.

A   A schematic diagram indicates sequence features of Lilli and the AFF proteins (Nilson *et al*, 1997; Wittwer *et al*, 2001). A correspondence is seen between the C-terminal half of Lilli and the C-terminal two-thirds of the AFFs (the Lilli-like segment). Scale bar indicates length in amino acids (a.a.). pSer, poly-serine domain; NLS, nuclear localization sequence; CHD, C-terminal homology domain; POU, POU transactivation domain; AT, AT-hook DNA-binding motif; NHD, N-terminal homology domain; ALF, AF4/LAF4/FMR2 homology domain.

B–E   AFF4 (green) and FOXN1 (red) are shown by immunofluorescence in the following wild-type tissue samples: (B) murine hair follicles, P9; (C) developing murine epidermis, E16.5; (D) human epidermis, adult; (E) murine thymus, P0, outer region. DNA is stained by Hoechst dye 33258 (blue). Co-localization of AFF4 and FOXN1 generates yellow color, visible in cell nuclei of all samples. In panel C, the fluorescent signal in the periderm (P) is nonspecific, as it is present when primary antibodies are omitted from the staining. Inner regions of the murine thymus (not shown) yielded the same extensive overlap of FOXN1 and AFF4 staining as that shown in panel E. Arrowheads mark the dermal/epidermal border (C, D). CH, cortex of the hair; CT, cortex of the thymus. Scale bars, 20 μm.

nude mice, the *Aff4* mutants developed bald skin, with the hairlessness extending over much of the body (Fig 4B–D). In conjunction with this coat defect, *Aff4* mutants displayed fewer and shorter vibrissae (whiskers) than normal animals, with the external vibrissae appearing bent or wavy, again analogous to nude mice (Fig 4E–G). Coat and vibrissal defects were observed in all *Aff4* mutants and were the only abnormalities grossly visible, as the mutants otherwise appeared vigorous, reached adulthood, and generated offspring, once more similar to nude mice.

Nude mice appear bald due to a distinctive weakening of the hair shaft, as their hairs, though normal in number and possessing all standard cell types, lack rigidity, bend repeatedly, and break easily (reviewed in Mecklenburg *et al*, 2005). The extent of bending and

time of breakage vary from one hair fiber to the next in a given animal. A majority of nude-mutant hairs bend and break inside their hair canals as they grow, never extending much or at all above the skin. A sturdier minority of hairs grow well beyond the skin's surface and break inside their follicles during catagen, a post-growth period in which hair follicles shorten and hairs are forcibly moved to a more superficial position. Once a hair fiber breaks, its pieces accumulate in the hair canal, causing the canal walls to swell outward.

The alopecia of the *Aff4* mutants likewise resulted from a weakening of the hair shaft. In *Aff4*-mutant skin, hair shafts bent and broke inside their hair follicles, and the bent, broken shafts then caused the canals to dilate (Fig 4H–K). Occasionally, hair shafts

Figure 4.

Figure 4. AFF4 and FOXN1 play similar roles in the skin.

A A schematic diagram shows the design of the $Aff4^{flox}$ allele and the strategy for knocking out AFF4. The deletion of exons 10 and 11 ablates AFF4's entire Lilli-like segment.

B–N Representative skin phenotypes of wild-type (WT), $Foxn1^{nu/nu}$ (Nude), or $KRT14$-cre; $Aff4^{flox/flox}$ (Aff4 cko) mice are shown macroscopically (B-G) or histologically after hematoxylin and eosin staining (H-N). The phenotypes compared are as follows: (B-D) hair coats, 4-month-old adults; (E-G) vibrissae, P7; (H) hair follicles with growing hairs, juveniles; (I-K) regressing hair follicles, juveniles; (L-N) epidermis, P9. In panel (H), micrographs from left to right are WT, Nude, and Aff4 cko. In panels (I-K), HF marks examples of hair follicles. In panels (L, M), arrowheads indicate the dermal/epidermal border; arrows mark examples of bent hair shafts. Scale bars: (H, L-N), 20 μm; (I-K), 40 μm.

broke while they grew (Fig 4H), thus mimicking the majority of nude hairs. More frequently, hair broke during catagen (Fig 4I–K), as hair shafts generally grew beyond the skin surface. This sequence of hair growth, breakage, and loss was repeated periodically in the *Aff4* mutants, as it is in nude mutants, suggesting that hair follicles of both mutants can proceed cyclically through growth (anagen) and post-growth (catagen, telogen) phases much as normal hair follicles do. Concomitantly, less hair became visible in both mutants with increasing age or hair-cycle number, consistent with the bent, broken hairs eventually impairing anagen. In sum, *Aff4* mutants, like nude mutants, produced hair shafts with a range of structural weaknesses, and the two mutant ranges overlapped, with much of the *Aff4*-mutant hair behaving like the sturdiest nude-mutant hair and breaking in catagen.

The *Aff4* mutants also resembled nude mutants in their epidermis, as the epidermis of both mutants underwent a thickening of the suprabasal, differentiating layers (Fig 4L–N). Consistent with their skin phenotypes, $KRT14$-cre; $Aff4^{flox/flox}$ mice displayed few, if any, cutaneous epithelial cells positive for the AFF4 protein (Fig EV3), confirming that these mice were conditional knockouts (*Aff4*-cko mice). Thus in the skin, a deficiency of AFF4 produced defects similar to a deficiency of FOXN1, suggesting that AFF4 and FOXN1 share a common mechanism of action and showing that they serve a common purpose.

AFF4 and the morphogenesis of the thymus

Foxn1 is activated near the start of thymus development, and hence to ablate *Aff4* in the developing thymus before FOXN1 begins to function, the $Aff4^{flox}$ allele was converted to a germline $Aff4^{ko}$ allele (see Materials and Methods). $Aff4^{+/ko}$ heterozygotes appeared normal in all respects, showing that $Aff4^{ko}$ is recessive to $Aff4^+$ and hence that haploid $Aff4^+$ is ordinarily sufficient to fulfill *Aff4*'s functions. On certain strain backgrounds, haploid $Foxn1^+$ has been reported to yield modest decreases in thymus size in juveniles (Kojima *et al*, 1984), but in our colony, mice heterozygous for $Foxn1^+$ and a nude allele appear to develop normally (Fig EV4), generating thymi equivalent in size to $Foxn1^{+/+}$ and thus classifying nude alleles as recessive to $Foxn1^+$ during organogenesis.

$Aff4^{ko/ko}$ newborns (P0) lacked visible vibrissae but had otherwise normal external morphology, making them similar to nude newborns, which likewise lack vibrissae but appear otherwise normal externally. The $Aff4^{ko/ko}$ newborns also resembled certain $Aff4^{-/-}$ newborns (Urano *et al*, 2005), as they died at or shortly after birth but had no clear cause of death (this lethal phenotype was fully penetrant in $Aff4^{ko/ko}$ mice). Shortly before birth (E18.5), $Aff4^{ko/ko}$ embryos were alive and present at approximately Mendelian frequencies, leading us to focus on the E18.5 time point.

As shown in Fig 5A, $Aff4^{ko/ko}$ $Foxn1^{+/+}$ embryos exhibited thymic hypoplasia, and this hypoplasia became more severe in $Aff4^{ko/ko}$ $Foxn1^{+/-}$ embryos, as the knockout/nude allele $Foxn1^-$ (Nehls *et al*, 1996) synergized with the *Aff4* knockout. This synergy was likewise observed in $Aff4^{+/ko}$ $Foxn1^{+/-}$ embryos, which exhibited a small-thymus phenotype similar to that of $Aff4^{ko/ko}$ $Foxn1^{+/+}$ embryos (not shown). The thymic hypoplasia appeared to result from an impairment of thymic growth, rather than a failure of thymic differentiation or cell survival, as the thymi were not missing any major components (e.g., cortex or medulla), showed no obvious changes in the expression of various differentiation markers (Appendix Table S1), and did not exhibit an increase in apoptosis (as judged by TUNEL staining; unpublished observation). Given the correlation between the extent of thymic hypoplasia and the number of *Foxn1/Aff4* mutant alleles, the results suggest that FOXN1 and AFF4 function together in the same growth-promoting mechanism, that this mechanism is weakened but still largely sufficient when one of the four *Foxn1/Aff4* alleles is inactivated, and that this mechanism becomes clearly insufficient when a second allele (any allele) is inactivated, leading to thymic abnormalities.

Similar to $Aff4^{ko/ko}$ animals, mice homozygous for the hypomorphic $Foxn1^R$ allele exhibit thymi that are reduced in size but normal in histology (Nowell *et al*, 2011). Hence, a large but incomplete loss of *Foxn1* function has effects resembling the ablation of *Aff4*. Nude mutants display a more severe thymic hypoplasia, as they arrest thymic growth, differentiation, and development overall after generating a properly positioned thymic primordium, the small, epithelial, lobular precursor of the thymus (Blackburn *et al*, 1996; Nehls *et al*, 1996; and references therein). Conversely, gains of FOXN1 function induce the growth and differentiation of new thymic tissue (Bredenkamp *et al*, 2014a; Bredenkamp *et al*, 2014b), and following thymic organogenesis, FOXN1 normally shapes and maintains thymic size, structure, and cell types (Su *et al*, 2003; Chen *et al*, 2009; Cheng *et al*, 2010; Zook *et al*, 2011). As such, FOXN1 promotes a broad range of thymic processes—growth, differentiation, and maintenance (see Vaidya *et al*, 2016 for review)—and a subset of these processes, related in particular to growth, appear to be facilitated by AFF4. The mechanism by which FOXN1 promotes thymic growth and development is not well understood but most likely employs *Dll4*, which encodes a juxtacrine signaling protein, is upregulated directly by FOXN1 in thymic epithelial cells (Bajoghli *et al*, 2009; Nowell *et al*, 2011; Bredenkamp *et al*, 2014b; Zuklys *et al*, 2016), and itself promotes thymic growth and development, as the ablation of *Dll4* in thymic epithelium reduces thymic cellularity (Hozumi *et al*, 2008; Koch *et al*, 2008). DLL4 did not clearly diverge from its normal staining pattern in the thymi of $Aff4^{ko/ko}$ $Foxn1^{+/+}$ mice but was significantly reduced in the thymic epithelium of $Aff4^{ko/ko}$ $Foxn1^{+/-}$ mice (Fig 5B and C), suggesting that the
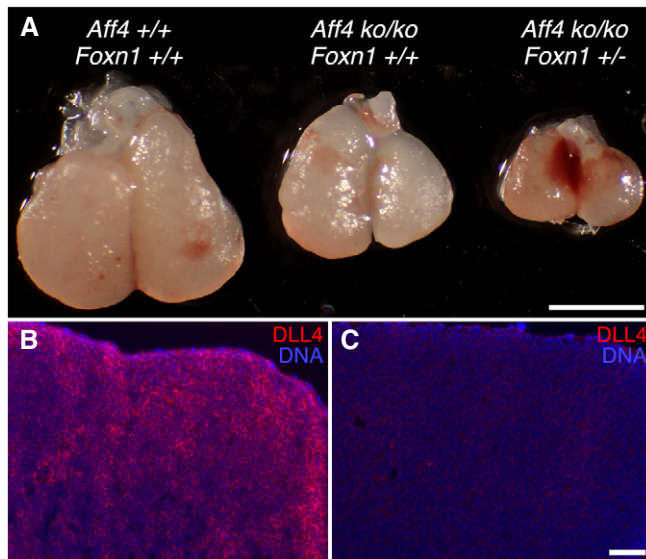
Figure 5. AFF4 and FOXN1 play cooperative roles in the thymus.

A–C Thymi from E18.5 embryos are shown: (A) intact with genotypes indicated, or (B, C) after sectioning, immunofluorescent staining for DLL4 (red), and counterstaining of DNA (blue). Sectioned samples are wild-type (B) or *Aff4*$^{ko/ko}$; *Foxn1*$^{+/-}$ (C). Scale bars: (A), 1 mm; (B-C), 50 μm.

synergistic hypoplasia of the *Aff4*$^{ko/ko}$ *Foxn1*$^{+/-}$ double mutants resulted in part from a decrease in DLL4.

Overall, in the thymus as in the skin, *Aff4* and *Foxn1* yield related but hierarchical phenotypes, with *Foxn1* having the greater phenotypic impact. Consistent with such effects, *Aff4/Foxn1* double knockouts (*Aff4*$^{ko/ko}$ *Foxn1*$^{-/-}$ or *KRT14-cre; Aff4*$^{flox/flox}$ *Foxn1*$^{-/-}$ mice) were identical to *Foxn1* knockouts (*Foxn1*$^{-/-}$; nude mutants) in their thymic and cutaneous phenotypes (not shown). Hence, while heterozygous nude mutations were synergistic with *Aff4* mutations, homozygous nude mutations were epistatic to *Aff4* mutations. In all, the results show that AFF4 promotes many of the same developmental processes as FOXN1 and suggest that AFF4 largely performs this function by facilitating a component of FOXN1 function.

AFF4 and FOXN1 in gene regulation

We next investigated the mechanism by which AFF4 and FOXN1 interact and as a starting point examined whether *Foxn1* affects the expression pattern of *Aff4* or vice versa. As judged by the immunofluorescent staining of skin sections, AFF4 levels and distribution were normal in *Foxn1*-null mice, and FOXN1 levels and distribution were normal in *Aff4*-cko mice (unpublished results), suggesting that neither protein regulates the amount or location of the other.

To assess the effects of AFF4 and FOXN1 on global gene expression, skin from wild-type, *Foxn1*-null, or *Aff4*-cko mice was analyzed by RNA-seq at a time when the animals were attempting to grow their first hair coats. Consistent with the similar phenotypes of the *Aff4* and *Foxn1* mutants, AFF4 and FOXN1 had broadly similar effects on the transcriptome, as RNA-seq identified 708 genes that were downregulated in both mutants and 454 genes that were

upregulated in both mutants (Fig 6A, Datasets EV1–EV3). *Aff4* and *Foxn1* were notably independent of each other's wide-ranging effects, as the *Aff4* mutant expressed *Foxn1* at normal levels, and the *Foxn1* mutant expressed *Aff4* at normal levels (Datasets EV1–EV3), suggesting that neither gene regulates the other. Of the many differentially expressed genes uncovered, a specific subset stood out for their relevance to the mutants' morphological defects.

A hair is principally a cross-linked mass of filaments and interfilamentous matrix, with the filaments composed of keratins (mostly cysteine-rich hair keratins) and the matrix composed of cysteine-rich keratin-associated proteins (KRTAPs). Of the genes downregulated in both the *Aff4* and *Foxn1* mutants, 13 encoded hair keratins, 11 encoded other follicular keratins, and 46 encoded KRTAPs (Table EV1). Many of these keratin genes or *Krtap*s ranked among the most strongly downregulated genes of each mutant (Table EV1), and mutations in 9 of these keratins (murine or human) are known to produce fragile, misshapen, or sparse hair (Table EV1), defects consistent with those of the *Aff4/Foxn1* mutants. Likewise, 33 genes encoding other types of proteins—e.g., transcription factors, cell–cell junction components, signal-transduction mediators, or protein-modifying enzymes—were downregulated in both mutants and found, when mutated in mice or humans, to yield hair or epidermal abnormalities related to those of the *Aff4/Foxn1* mutants (Table 1). Hence, while no single downregulated gene has produced a phenotype identical to the *Aff4/Foxn1* mutant phenotype, the collective downregulation of these 24 keratin genes, 46 *Krtap*s, and 33 other genes is most likely responsible in large part for the bent, broken hair shafts and other defects of the *Aff4/Foxn1* mutants. Furthermore, as the defects of the mutants appear to result principally from the downregulation of genes, the results provide further evidence of FOXN1 and AFF4 serving primarily as activators of transcription and developmental programs.

Other genes downregulated in both mutants included genes that promote pigmentation or cell polarization (Appendix Table S2), processes of clear importance to cutaneous epithelia (McNeill, 2010; Kirschner & Brandner, 2012; Niessen *et al*, 2012; Reissmann & Ludwig, 2013; Weiner *et al*, 2014; Liao *et al*, 2017; and references therein). Most of the downregulated pro-pigmentation genes—*Mitf*, *Tyr*, and *Oca2*—are specifically expressed in melanocytes, whereas the remaining pro-pigmentation gene, *Kitl*, is expressed in epithelial cells of the developing hair shaft and encodes an extracellular signaling protein (Reissmann & Ludwig, 2013; Liao *et al*, 2017; and references therein), suggesting that decreased *Kitl* expression in FOXN1/AFF4-deficient cells led to decreased *Mitf*, *Tyr*, and *Oca2* expression in melanocytes. The differentially expressed transcripts of the mutants did not appear to include a reported circular *Aff4* RNA, which is composed of exons 2–5, was detected by others in various types of cells (Memczak *et al*, 2013; Rybak-Wolf *et al*, 2015; Mi *et al*, 2019) and as judged by semi-quantitative RT–PCR exhibited comparable levels of expression in wild-type, *Aff4*-cko, and *Foxn1*-null skin.

Overall, there was substantial overlap in *Foxn1*- and *Aff4*-dependent gene expression, as 40% of the genes downregulated in the *Foxn1*-null mutant were downregulated in the *Aff4*-cko mutant, and 70% of the genes downregulated in the *Aff4*-cko mutant were downregulated in the *Foxn1*-null mutant (percentages are derived from Fig 6A). When genes were ranked by fold downregulation, even greater overlaps emerged (Fig 6B). Of the 100 genes most strongly
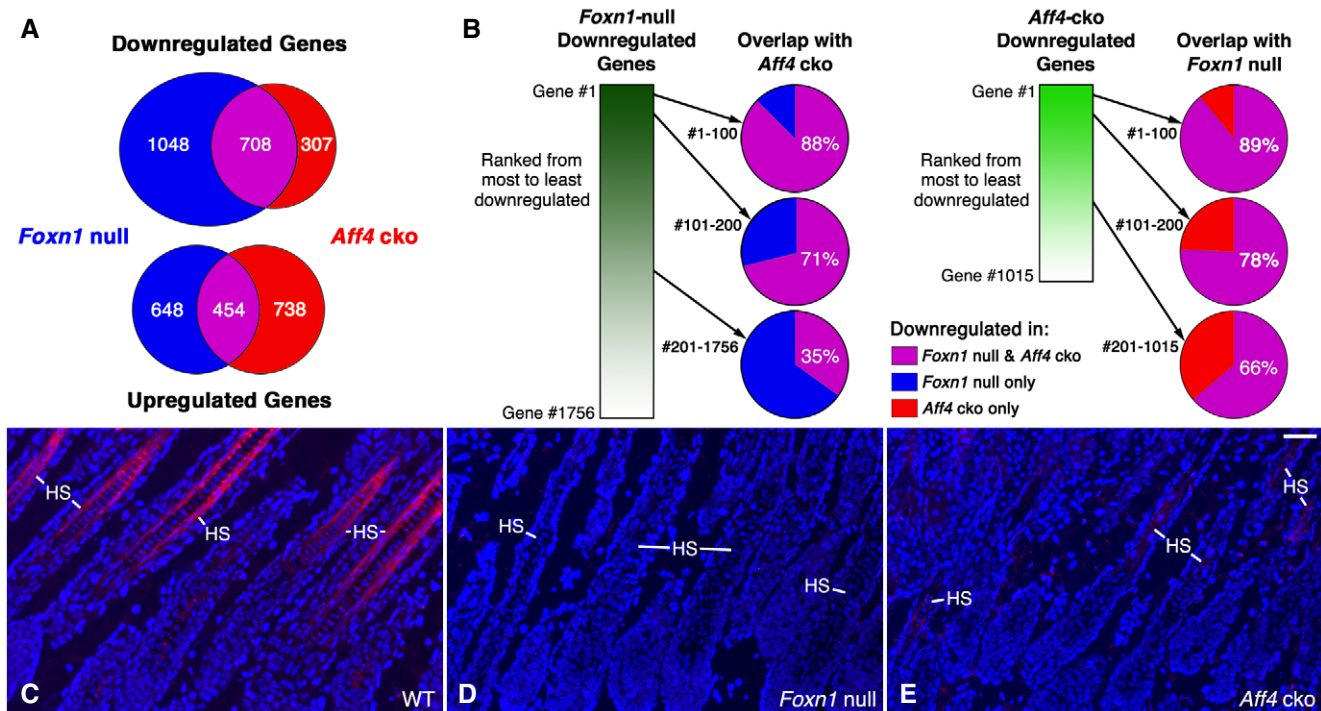
Figure 6. AFF4 and FOXN1 have similar effects on gene expression.

A   Venn diagrams summarize global changes in gene expression caused by the inactivation of *Foxn1* or *Aff4* and detected by RNA-seq in murine skin at P6. The upregulated or downregulated gene populations of each mutant—and the extents to which they overlap—are indicated.

B   Gradient bars (green) signify the ranking of downregulated genes by fold change, with genes ordered from most downregulated (gene #1) to least downregulated. Fold change was determined by RNA-seq. Separate rankings were performed for each mutant (*Foxn1* null or *Aff4* cko). Pie charts indicate whether genes of a given rank in one mutant were downregulated in the other mutant. Percentages indicate the overlap in the mutants' downregulated gene populations.

C–E   KRT86 (red) is shown by immunofluorescence in skin sections from wild-type (WT), *Foxn1* null, or *Aff4* cko mice at P9. DNA is stained blue. HS marks examples of hair shafts. Scale bar, 40 μm.

downregulated in the *Foxn1* mutant, 88 were downregulated in the *Aff4* mutant. More broadly, of the *Foxn1* null's 200 most downregulated genes, 80% were downregulated in the *Aff4* cko. These high overlap frequencies were reciprocal: Of the 100 or 200 genes most strongly downregulated by the loss of *Aff4* function, 89% and 84%, respectively, were downregulated by the loss of *Foxn1* function. Thus, the strongest effects of *Foxn1* appeared to be amplified by *Aff4*, and vice versa.

The keratin gene most strongly downregulated on average in the *Foxn1*-null and *Aff4*-cko mutants was *Krt86* (Table EV1), a gene known to be stimulated by FOXN1 (Schlake *et al*, 2000; Schorpp *et al*, 2000) and to be strongly and principally expressed in the developing hair cortex, the site of the highest FOXN1 and AFF4 levels. Consistent with the large downregulation of the *Krt86* mRNA, the KRT86 protein greatly decreased in hair shafts when either AFF4 or FOXN1 was absent (Fig 6C–E), showing KRT86 to be highly dependent on the presence of both AFF4 and FOXN1. Mutations in human *KRT86* cause monilethrix (Winter *et al*, 1997), a disease characterized by brittle or fragile hair, defects consistent with the *Foxn1/Aff4*-mutant phenotype. Hence, several lines of evidence pointed to KRT86 as a key downstream effector of FOXN1 and AFF4.

To investigate the FOXN1/AFF4 regulatory mechanism, we used *Krt86* as a model, as its strong expression in FOXN1/AFF4-positive

skin cells allowed intact skin to serve as the system for analysis. As a first step, we examined wild-type, *Foxn1*-null, or *Aff4*-cko mice for their levels of *Krt86* pre-mRNA (mRNA with introns present), as cellular pre-mRNA consists largely of transcripts in the act of being transcribed, making it a direct indicator of transcription (reviewed in Bentley, 2014). As shown in Fig 7A–C, *Krt86* pre-mRNA greatly decreased when FOXN1 or AFF4 was ablated in skin. The precise magnitude of the decrease fit well with the hierarchical genetic relationship of *Foxn1* and *Aff4*, as the *Foxn1* mutation, which produces a more severe or epistatic phenotype, had the larger effect on pre-mRNA levels. Notably, the pre-mRNA loss caused by each mutation did not become more severe as transcripts increased in length: Reductions in pre-mRNA were large and essentially equivalent at the first, ninth, and last exon/intron junctions. Thus, FOXN1 and AFF4 strongly promote the transcription of *Krt86* and exert their principal effects early in transcription, before *Krt86* transcripts elongate through the first exon/intron junction.

To determine whether FOXN1 and AFF4 promote *Krt86* transcription directly, the chromosomal *Krt86* locus was probed for bound FOXN1 or AFF4 by chromatin immunoprecipitation (ChIP) using skin from normal, *Foxn1*-null, or *Aff4*-cko mice and antibodies to FOXN1 or AFF4. A total of 25 chromatin sites were individually assayed—18 sites upstream of the transcription start site (TSS), 6 sites downstream of the TSS, and the TSS itself. The sites chosen

Table 1. FOXN1 and AFF4 cooperatively promote the expression of the developmental programs of the hair and epidermis.

Gene	Molecular function or process	Hair abnormalities			Epidermal abnormalities		PMIDs
		Fragile/Brittle	Misshapen/Malformed	Sparse/Bald	Hyperplasia	Acanthosis	
Braf	Signal-Transducing Kinase	●		●	●		16439621, 16474404, 16804887
Cdsn	Cell–Cell Junctions	●		●	●	●	12754508, 18436651, 19596793, 20691404
Cers4	Ceramide Synthesis			●			24738593
Ctnna1	Cell–Cell Junctions			●	●		11239416
Ctsl	Cysteine Protease			●	●	●	11023992
Cux1	Transcription Factor	●	●	●			11544187, 11839809
Dcaf17	Ubiquitination?			●			19026396
Dlx3	Transcription Factor		●	●	●	●	18684741, 21252474
Dsg4	Cell–Cell Junctions	●	●	●	●	●	12705872
Errfi1	Signal-Transduction Inhibitor				●		16648858
Foxq1	Transcription Factor		●				11309849
Fst	Signal Inhibitor		●		●		7885475
Gata3	Transcription Factor		●	●	●	●	12923059, 17151017
Gjb2	Cell–Cell Junctions/Communication			●	●		11912510, 20926451
Gjb6	Cell–Cell Junctions/Communication	●	●	●	●		11017065
Hoxc13	Transcription Factor	●	●	●			9420327, 21191399, 23063621
Lef1	Transcription Factor			●			7958926
Lgr4	Signal Receptor			●			18651655
Lpar6	Signal Receptor	●	●	●			18297070, 18297072
Padi3	Protein Citrullination		●				27866708
Prdm1	Transcription Factor				●	●	17846422, 25358790
Runx1	Transcription Factor		●				17011173
Scd1	Fatty Acid Synthesis			●	●	●	10545940
Sgk3	Signal-Transducing Kinase		●	●			15240817, 15871460
Sp6	Transcription Factor	●	●	●	●	●	18297738, 25344255
St14	Serine Protease	●	●	●	●	●	17273967, 17940283
Tchh	Structural Protein		●				27866708
Tgfa	Extracellular Signal		●				8477444, 8477445
Tgm3	Protein Cross-Linking	●	●				22496784, 27866708
Trps1	Transcription Factor			●			10615131, 12446778
Trpv3	Cation Channel		●				20403327
Zdhhc13	Protein Palmitoylation			●	●	●	20548961, 20548961
Zdhhc21	Protein Palmitoylation	●		●	●	●	19956733

The listed genes were downregulated in the skins of *Foxn1*-null and *Aff4*-cko mutant mice. Downregulation was determined by RNA-seq. Each listed gene, when mutated in humans or mice, yields abnormalities consistent with the abnormalities of *Foxn1*-null and *Aff4*-cko mutants: namely, fragile/brittle hair, misshapen/malformed hair shafts, sparse hair/bald skin, epidermal hyperplasia (an increase in the number of epidermal cells), and/or epidermal acanthosis (an increase in the number of spinous cells). The abnormalities resulting from mutations in each gene are indicated with closed circles. Mutant phenotypes were identified by searches of the OMIM and MGI databases using gene names; relevant PubMed IDs from the OMIM or MGI entries are indicated.

had obvious regulatory potential, such as conserved non-coding sequences (Frazer *et al*, 2004; Hardison & Taylor, 2012) or the region immediately upstream of the TSS. As shown in Fig 7D and E, FOXN1 and AFF4 bound to a chromatin element 2 kb upstream from the *Krt86* transcription start site. At this element, the binding of each protein was dependent in part on the other, as FOXN1 bound to a lesser extent when AFF4 was ablated, and AFF4 likewise bound to a lesser extent when FOXN1 was ablated (Fig 7F and G).
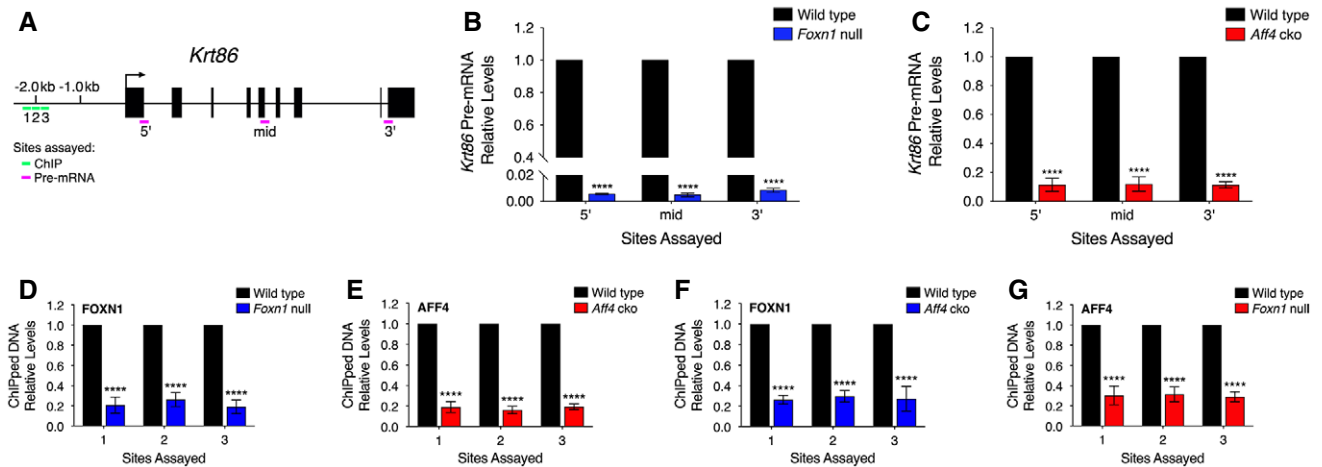
Figure 7. AFF4 and FOXN1 cooperatively activate transcription.

A   Murine *Krt86* is shown schematically with exons as rectangles and the transcription start site marked by an arrow. Sites assayed in the pre-mRNA or ChIP studies of panels B–G are indicated.

B–G   Graphs present pre-mRNA (B, C) or ChIP (D–G) assays of *Krt86* using skin from mutant mice (*Foxn1* null, *Aff4* cko) or corresponding wild-type controls at P6 (B, C) or P7 (D–G). ChIP assays were performed with antibodies to FOXN1 or AFF4 as indicated. All values are derived from 3 independent experiments and presented as mean ± S.D. Pre-mRNA measurements were analyzed statistically using two-way ANOVA with post hoc Sidak's multiple comparison test at a 95% confidence interval. ChIP assays were analyzed statistically using one-way ANOVA with post hoc Tukey's multiple comparison test at a 95% confidence interval. ****, $P \leq 0.0001$.

Consistent with these results, the CHD domain of AFF4 (see Fig 4A) was found *in vitro* to possess a large, positively charged surface and a substantial affinity for DNA (Chen & Cramer, 2019), suggesting that AFF4 is able to bind DNA directly. A similar though perhaps less stable FOXN1/AFF4 interaction was observed at the TSS, as AFF4 and FOXN1 were detected at the TSS, with the binding of each dependent on the other but with the binding of FOXN1 exhibiting greater fluctuation than AFF4 (Fig EV5). While binding to the same chromatin sites, FOXN1 and AFF4 did not discernibly co-immunoprecipitate as a soluble complex in assays performed *in vitro* (see Materials and Methods), suggesting that by themselves FOXN1 and AFF4 do not bind to each other and that one or more additional molecules mediate their interaction. In sum, FOXN1 and AFF4 bound in a reciprocally cooperative fashion in *cis* with and most likely at the *Krt86* core promoter, which requires both proteins for strong activity. These results suggest that FOXN1 and AFF4 are direct, synergistic activators of *Krt86*.

To understand how FOXN1 and AFF4 activate *Krt86* transcription, their effects on RNA polymerase II (Pol II) were assayed by ChIP using skin from normal, *Foxn1*-null, or *Aff4*-cko mice and antibodies to three different classes of Pol II—"total", P-Ser5, or P-Ser2 (antibodies to total Pol II recognize multiple isoforms). The P-Ser5 or P-Ser2 isoforms of Pol II are produced by phosphorylation after Pol II is recruited to a promoter and are associated generally with transcriptional initiation (P-Ser5) or elongation (P-Ser2) (reviewed in Jeronimo *et al*, 2016). As shown in Fig 8A–C, the ablation of FOXN1 or AFF4 caused dramatic decreases in total Pol II at the *Krt86* transcription start site as well as multiple sites downstream. Notably, in each mutant, the TSS and downstream sites exhibited essentially equivalent fold-decreases in Pol II, as Pol II appeared to be simply reduced across the gene, not halted just downstream of the TSS—and thus accumulating next to the TSS—due to pausing.

In all, this lack of Pol II suggests that Pol II was not recruited to *Krt86* and incorporated into pre-initiation complexes (PICs), the multifactor entities that place Pol II at a core promoter and facilitate initiation. Hence, the results suggest that FOXN1 and AFF4 promote and are critical for PIC formation, the first step of regulated transcription.

AFF4 did not clearly affect transcriptional steps following PIC formation at *Krt86*, as in the absence of AFF4, P-Ser5 Pol II and P-Ser2 Pol II underwent approximately the same fold decrease as total Pol II (Fig 8E and G). The loss of AFF4 therefore did not yield obvious defects in Pol II initiation, the release of paused Pol II, or Pol II elongation. Likewise, FOXN1 did not clearly affect P-Ser2 Pol II at *Krt86*, as in the absence of FOXN1, P-Ser2 Pol II decreased to the same extent proportionally as total Pol II (Fig 8F). However, across *Krt86* in the *Foxn1*-null mutant, P-Ser5 Pol II exhibited a clearly greater fold decrease than total Pol II (Fig 8D). This decline in P-Ser5 Pol II suggests that one or more of the following conditions arose in FOXN1's absence: a decrease in Ser5 phosphorylation, an increase in Ser5 dephosphorylation, or the masking of P-Ser5. In all cases, the decline reveals the existence of a transcriptional defect that is downstream of PIC formation and a specific result of the loss of FOXN1 function. Hence, following PIC formation and independently of AFF4, FOXN1 promoted at least one additional step of transcription. This step appeared unnecessary for Ser-2 phosphorylation but important for the production of transcript, as *Krt86* pre-mRNA declined to a substantially greater extent in the *Foxn1*-null mutant than in the *Aff4* mutant.

Taken together, the molecular results explain in large part the phenotypic results, namely why *Aff4* and *Foxn1* yield phenotypes that are different in degree but similar in kind. AFF4 stimulated one step of transcription (PIC formation) while FOXN1 stimulated two steps (PIC formation and a later step), enabling FOXN1 to make a
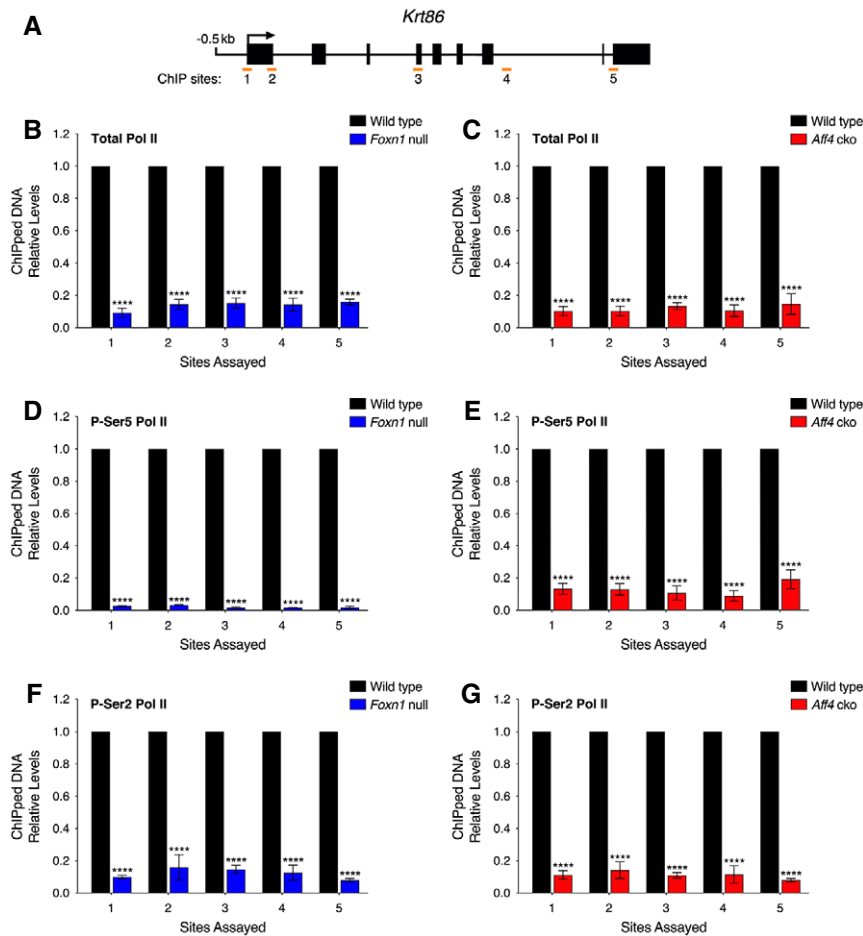
Figure 8. AFF4 and FOXN1 cooperatively promote pre-initiation complex formation.

A Murine *Krt86* is shown schematically as in Fig 7A. Sites assayed in ChIPs of panels B-G are indicated.

B–G Graphs present ChIP assays of *Krt86* using antibodies to total (B, C), P-Ser5 (D, E), or P-Ser2 (F, G) Pol II and skin from mutant mice (*Foxn1* null, *Aff4* cko) or corresponding wild-type controls at P7. All values are derived from at least 3 independent experiments and presented as mean ± S.D. Assay results were analyzed statistically using one-way ANOVA with post hoc Tukey's multiple comparison test at a 95% confidence interval. ****$P \leq 0.0001$.

greater impact on transcription and cutaneous/thymic phenotypes. Concomitantly, AFF4 stimulated one of the same transcriptional steps as FOXN1 (PIC formation)—the first step of FOXN1's mechanism of action—enabling AFF4 to make a considerable impact on FOXN1-dependent transcriptional programs and phenotypes. AFF4 is thus a regulatory partner of FOXN1, the first such partner to be identified.

Discussion

The goal of the present study was to find nude-like loci without screening mutant mice for nude-like phenotypes. Using flies as stand-ins, the study identified *Aff4*, a gene that promotes the development of a rigid, visible hair coat as *Foxn1* does, stimulates the growth of the thymus as *Foxn1* does, yields loss-of-function phenotypes similar to *Foxn1* loss-of-function phenotypes (null or hypomorphic), and serves as a partner to *Foxn1* in gene regulation. *Aff4*

thus performs functions like those of *Foxn1*, the nude locus, making it the first nude-like locus found since the nude locus was discovered 54 years ago. Clearly, *Aff4* is not simply a partner of *Foxn1*—it evolved other roles as well (see below). Nonetheless, if mutant mice had been screened for nude-like loci (rather than flies), *Aff4* is a gene that would have been isolated. Hence, though the fly can never have a nude-like phenotype, it can become a model for this phenotype under the right circumstances.

Molecular and cellular roles of AFF4

In previous studies, the molecular biology of AFF4 was investigated using cell-culture or cell-free systems. These systems revealed that AFF4 promotes the elongation phase of transcription by assembling around itself a collection of potent elongation factors, specifically, P-TEFb, ENL, and/or ELL factors (Estable *et al*, 2002; Mueller *et al*, 2007; He *et al*, 2010; Lin *et al*, 2010; Sobhian *et al*, 2010; Yokoyama *et al*, 2010). These AFF4-nucleated complexes, termed "super

elongation complexes" (SEC; Lin *et al*, 2010), "AEP" (<u>A</u>F4 family/ <u>E</u>NL family/<u>P</u>-TEFb; (Yokoyama *et al*, 2010)), or '"EAP' (<u>e</u>longation <u>a</u>ssisting <u>p</u>roteins; Mueller *et al*, 2007; Mueller *et al*, 2009), directly stimulate the expression of large sets of genes in various cell-culture systems under a variety of conditions (Lin *et al*, 2011; Luo *et al*, 2012). Consequently, AFF4 is often thought to facilitate gene expression globally and to do so as a scaffold within broadly or generally used machinery for elongation (Jonkers & Lis, 2015; Chen *et al*, 2018; Core & Adelman, 2019).

Here, we investigated the role of AFF4 in animals and uncovered a new function for this transcription factor: namely, that AFF4 promotes the first step of regulated transcription, the formation of pre-initiation complexes, and does so in partnership with a specialized transcription factor, FOXN1, so as to induce the development of a specific set of traits. Mechanistically, these findings are in accord with previous studies of AFF1, which suggested that AFF1, while bound to AEP components, promotes PIC formation at MLL targets and that PIC formation is the rate-limiting step of AFF1 function (Okuda *et al*, 2015; Okuda *et al*, 2016; Yokoyama, 2018). In the case of our model gene *Krt86*, which is strongly activated by AFF4, AFF4 did not clearly regulate transcriptional events downstream of PIC formation, such as initiation, pausing, or elongation. Moreover, as shown here, the ablation of AFF4 in mice generated focused phenotypes, as the conditional and germline AFF4 knockouts appeared well developed overall and exhibited relatively few clear defects, which often recapitulated the defects of FOXN1 mutants. The AFF4 knockouts did not display a substantial rate of embryonic mortality, an extensive disruption of development, broadly aberrant morphology, or large-scale cell death, abnormalities that would be expected if a broad or general regulator of transcription was lost. The AFF4 knockouts contrasted markedly with cyclin T2 knockouts, for example, which die prior to the 4-cell stage of embryonic development (Kohoutek *et al*, 2009). Cyclin T2 is a component of some but not all P-TEFb, which in turn is just one of several elongation factors in the SEC and is thought to perform its function largely through the SEC (Chen *et al*, 2018; Core & Adelman, 2019).

One unifying explanation for the *in vitro* and *in vivo* results is as follows: AFF4 plays two basic roles in transcription, one broad/ general (like that of P-TEFb), and the other specific (like that of FOXN1). The broad/general role is redundant or weak in impact, rendering AFF4 dispensable in many cells where it appears. The specific role, in contrast, is unique and has a substantial impact on defined phenotypes.

While this explanation accounts for the data, we note that AFF4-positive elongation complexes have been detected and studied primarily in contexts that are pathological or stressful, such as hypoxia (Galbraith *et al*, 2013), oncogenic protein production (Lin *et al*, 2010; Yokoyama *et al*, 2010), high temperature (Lin *et al*, 2010; Luo *et al*, 2012), growth factor starvation/stimulation procedures (Lin *et al*, 2011; Gardini *et al*, 2014), cell lines derived from cancerous (often metastatic) tumors (Liang *et al*, 2018; Dahl *et al*, 2020), or the transcription of viruses, specifically, human immunodeficiency virus-1, herpes simplex virus-1, or hepatitis B virus (Niedzielski *et al*, 2007; He *et al*, 2010; Sobhian *et al*, 2010; Alfonso-Dunn *et al*, 2017; Francisco *et al*, 2017). This apparent association between AFF4 activity and abnormal cellular conditions suggests another unifying explanation: that AFF4 plays exclusively specific roles in cells, but one of these specific roles is to cope with a general

problem, such as stress or cellular damage. In this scenario, AFF4 is present but largely inactive in cells until it is mobilized by certain developmental programs (e.g., hair, epidermis, thymus) or stresses (e.g., hypoxia, heat, viral infection) for a specific purpose, namely to activate morphogenetic genes or to mitigate the cellular stress. In some cases, AFF4 may be used for both purposes: For example, a virus-infected cell may mobilize AFF4 to cope with the stress of infection; the virus may then hijack AFF4 to activate its own morphogenetic program (Alfonso-Dunn *et al*, 2017; Francisco *et al*, 2017). Notably, AFF4 was dispensable in most if not all of the FOXN1-negative skin cells in which it appeared, consistent with AFF4 waiting for a mobilizing event in those cells. Presumably, once mobilized, AFF4 promotes Pol II transcription at steps determined in large part by the mobilizing factors.

Flash-forward genetics

In previous studies, the sequences of FOX family members were compared across various animal groups, and FOXN1 was found to be unique to vertebrates (Bajoghli *et al*, 2009). The thymus likewise is unique to vertebrates, while hair is unique to mammals. In the fish *Oryzias latipes*, homozygous null mutations in *foxn1* lead to a smaller but functional thymus (Swann *et al*, 2014). In the amphibian *Xenopus tropicalis,* loss-of-function mutations in *Foxn1* result in the absence of a thymus (Nakai *et al*, 2016). FOXN1 itself has changed significantly over the course of vertebrate evolution, as the FOXN1 proteins of *Oryzias*, *Xenopus*, and reptiles/birds display identities to murine FOXN1 of 25, 46 and ~55%, respectively.

Taking these observations together, a basic evolutionary narrative is suggested. In the common ancestors of modern vertebrates, *Foxn1* arose as a genetic novelty and was recruited to promote the development of the thymus, a phenotypic novelty (Bajoghli *et al*, 2009; Swann *et al*, 2014). In the common ancestors of modern tetrapods, *Foxn1* evolved in sequence and function and became essential for the development of the thymus. In the common ancestors of modern mammals, *Foxn1* further evolved in sequence and function, became essential for another phenotypic novelty, hair, and thus became central to a molecular novelty, the mechanism underlying the nude phenotype. This entire series of novelties arose after mammals and flies last shared a common ancestor. Hence, when FOXN1 interacted with Lilli and reproduced a regulatory module that specifically promotes the creation of the hair and thymus in mammals, the fly became at least a partial model for innovations accumulated by a distant lineage, in a sense experiencing a "flash-forward" along another evolutionary path. As this flash-forward was revealed by a distinct kind of forward genetics, the approach has been named "flash-forward genetics" and should facilitate the elucidation of other traits to which traditional genetics are difficult to apply.

Biological models have always been expected to possess an obvious likeness to the phenomena they seek to model. And when tractable likenesses are lacking and the genetic dissection of a trait appears unfeasible, the logical approach has been to pursue a molecular dissection of the trait, often via elegant techniques such as RNA-seq, ChIP-seq, microarray analyses, the yeast two-hybrid system, or the affinity purification/mass spectrometry of molecular complexes. These techniques have yielded invaluable, extremely detailed pictures of the molecular events inside cells, and one consistent part of these pictures is that single molecules routinely

interact with large numbers of others, at times thousands of others. For example, in the RNA-seq analysis presented here, FOXN1 was found to affect the expression of 2,858 genes, directly or indirectly. And FOXN1 is just one actor in the traits that it promotes: Each FOXN1-interacting molecule may interact with thousands of molecules (AFF4 affected 2,207 genes); and each of these thousands of molecules may interact with thousands of molecules, and so on. Even the simplest trait arises in a torrent of molecular interactions. Obvious questions arise: Do all of these interactions matter? Are they all the product of selection? Presumably, some interactions are more important than others.

In the present study, we sought to find what matters for the function of FOXN1 and the development of the mammalian skin and thymus. As such, we generated a FOXN1-based genetic model using a robust tractable organism (the fruit fly) that could present FOXN1 with a large variety of relevant molecules (molecules found in mammals), clearly display FOXN1's output, and set a meaningful threshold for the display of FOXN1's output, as a robust living system should possess strong homeostatic mechanisms and use them to buffer out the "noise" or less potent actions of FOXN1.

And rather than screen this model for an obvious likeness or a phenotype per se, we screened for interactions characterized by synergy, effectivity, and a resulting power to disrupt. Interactions that turned small changes in one molecule into large changes in the morphology and fitness of the animal were expected to be manifesting their functionality and selection. Certainly, interactions with such properties usually have selected-for functions. And as selection only operates on interactions that matter—as interactions must substantially affect survival or reproduction to be subject to selection—the isolated interactions were predicted to be significant, not only for the function of FOXN1, but also for mammals generally. The results of the screen support the underlying logic: The interaction between FOXN1 and AFF4/Lilli proved to have a beneficial function in mammals and was surely selected for. The synergy, effectivity, and resulting disruptive power of the interaction were telltale signs and consequences of multimolecular positive selection. Potentially, the genetic approach used here can be carried out successfully with other tractable transgenic systems, including cultured cells, with insertional mutagenesis providing the single-copy (weak) loss-of-function mutations. Ultimately, the approach may facilitate the dissection of virtually any mechanism that evolved through selection, including the mechanisms that drive cancer, as cancer arises through the selection and evolution of mutant cell populations, and flash-forward genetics should identify interactions that were selected for as a cancer evolved.

In the fly, FOXN1 also undoubtedly interacted with molecules in ways that were not selected for, and these purposeless interactions were presumably numerous, as FOXN1 broadly affected the characteristics of the ommatidia (FOXN1 affected ommatidial differentiation, number, and location) and most likely did so in part by binding to and altering the expression of genes that it did not evolve to regulate, genes not among its selected-for targets in mammals. All of this purposeless activity may seem unrepresentative of living systems—the molecular interactions found in normal cells are generally assumed to serve purposes, particularly when the interactions are specific and reproducible. In fact, interactomes may not be so well honed by selection, as biological molecules appear to engage routinely in interactions that are specific, reproducible, and purposeless. For example, there is evidence that transcription factors normally bind to chromosomal sites simply because the sites fortuitously match their recognition sequences, not because the binding yields beneficial effects on gene expression (reviewed in Biggin, 2011). Likewise, there is evidence that kinases and metabolic enzymes modify molecules (e.g., phosphorylate proteins) simply because the molecules fortuitously match their substrate requirements, not because the modifications confer physiological benefits (Landry *et al*, 2009; Khersonsky & Tawfik, 2010). Such purposeless interactions appear to be by-products of selection, that is, the result of selection for other interactions (Gould & Lewontin, 1979; Gould, 1997). Purposeless interactions may also be products strictly of chance, fixed into populations or species by genetic drift. In all cases, these interactions presumably persist because they evade negative selection—their individual costs are not great enough to reduce survival and reproduction. They lack the impact needed to be selectable and by this standard do not matter.

Hence, like the FOXN1 fly model, normal cells appear to engage in purposeless activity and to do so by design, as their genes program them to do it. Only some specific molecular interactions appear selected for. The results presented here suggest that selected-for interactions can be distinguished by certain portable or inherent properties, in particular, synergy and effectivity, which render them potently advantageous in their normal (evolutionary) circumstances and potently disruptive in abnormal circumstances. Accordingly, screening for the powerfully disruptive is a way to screen for the powerfully advantageous. And sowing chaos in a tractable system (flies) is a way to model an adaptive trait of "intractable" organisms (mammals). This modeling by disruption pinpoints important interactions through their distinct capacity to injure and—as shown here for the skin, thymus, and FOXN1 pathway—can reveal vital mammalian mechanisms through in essence a biological irony: The more harmful an interaction is to flies, the more beneficial it is to mammals.

Materials and Methods

FOXN1 fly model

Flies were raised on cornmeal-dextrose-yeast medium, and the cultivation temperature was 25°C, except as indicated for the manipulation of *hs-GAL4* activity. Males and females were analyzed in every experiment, except for the suppressor screen of the X chromosome, when females typically were analyzed (see "Fly suppressor screen"). Except where indicated, fly strains were obtained from the Bloomington *Drosophila* Stock Center.

The *UAS-Foxn1* transgene was constructed by cloning a murine *Foxn1* cDNA (nucleotides 53-2135) into the *Eco*R I and *Kpn* I sites of the P-element transgenesis vector pUAST, creating pW7. The *Foxn1* cDNA contained the complete coding sequence of the wild-type, 648-amino acid FOXN1 protein. To generate *UAS-Foxn1* transgenic flies, pW7 was injected with helper plasmid Δ2-3 into y^1 w^{67c23} embryos at the Cutaneous Biology Research Center Transgenic Fly Core. Transformation of flies to w^+ (a marker carried by pUAST) indicated successful transgenesis. In all transgenic experiments, transgenic phenotypes were analyzed with each transgene present in a hemizygous condition.

Six independent lines of *UAS-Foxn1* transgenic flies were generated (IS85 1-6). Males from each *UAS-Foxn1* line were crossed to w^1; *sna^{Sco}/SM1; MKRS/TM2* females to determine the chromosome on which the transgene had inserted. Males from 3 *UAS-Foxn1* lines (IS85 4-6) were also crossed to *GMR-GAL4* females to assess *UAS-Foxn1* expression and phenotypic consequences. All 3 *UAS-Foxn1* lines generated rough eyes when *GMR-GAL4* was present. One *UAS-Foxn1* line (IS85 4) was chosen for the suppressor screen and other studies. This line carried *UAS-Foxn1* on chromosome 2.

Fly suppressor screen

The screen employed a *GMR-GAL4* transgene that had inserted on chromosome 2 (like the *UAS-Foxn1* transgene). Prior to the start of the screen, the *GMR-GAL4* and *UAS-Foxn1* transgenes were linked together on the same chromosome by crossing *GMR-GAL4/UAS-Foxn1* females to *sna^{Sco}/SM1* males and isolating *GMR-GAL4 UAS-Foxn1/SM1* spontaneous recombinants.

The primary screen for FOXN1 suppressors was conducted by crossing *GMR-GAL4 UAS-Foxn1/SM1* flies to individual fly strains of the Bloomington Complete Deficiency Kit, a collection of deletion (deficiency; *Df*) stocks providing coverage of the X chromosome and the three autosomes. Progeny of these crosses were scored for suppression (rescue) of the rough-eye phenotype induced by *GMR-GAL4 UAS-Foxn1*. Screening procedures were generally as follows. To screen X chromosome deficiencies (*Df(1)*), *GMR-GAL4 UAS-Foxn1/SM1* males were mated to *Df(1)/balancer* females. Female *GMR-GAL4 UAS-Foxn1* progeny were scored, with those receiving the deficiency compared to those receiving the X balancer. To screen autosomal deficiencies, *GMR-GAL4 UAS-Foxn1/SM1* females were crossed to *Df/balancer* males. Male and female *GMR-GAL4 UAS-Foxn1* progeny were scored, with those receiving the deficiency compared to those receiving its paired balancer. The deficiencies were thus screened in a hemizygous condition. A total of 9 suppressors were identified.

The suppressors isolated in the primary screen were tested for FOXN1 specificity by crossing suppressor-positive *Df/balancer* flies to *GMR-p21* flies. *GMR-p21* progeny were then scored for suppression of the p21 rough-eye phenotype (*Df* versus balancer). Five suppressors of the FOXN1 eye phenotype were found to suppress the p21 eye phenotype and accordingly were ruled out as candidates for additional study.

jumu mutations were tested individually in a heterozygous condition for suppression of FOXN1 phenotypes. The basic genotype of tested flies was *GMR-GAL4* or *hs-GAL4/UAS-Foxn1; jumu* allele/*TM2*.

Suppressor mapping and identification

Suppressors isolated in the primary screen were mapped more precisely using overlapping deficiencies, i.e., fly strains carrying deletions known to overlap with the presumptive suppressor deletions. Each overlapping deficiency was tested individually for suppression of the FOXN1 rough-eye phenotype, and these tests followed the same procedures used in the primary screen. In the case of the presumptive suppressor *Df(2L)23C;23E3-6*, the following five overlapping deficiencies were tested (putative deleted segments appear in parentheses): *Df(2L)JS31* (23A3 to 23D6), *Df(2L)JS17*

(23C1 to 23E2), *Df(2L)C144* (22F4 to 23C3), *Df(2L)JS32* (23C3 to 23D2), and *Df(2L)S2590* (23D2 to 23E3). The first 3 deficiencies were suppressors, while the last 2 deficiencies were not suppressors, pinpointing the suppressor to 23C and most likely 23C1-3, a region with just 9 known genes.

To identify the specific suppressor gene(s), loss-of-function mutations in specific genes of region 23C were tested individually for suppression of the *GMR-GAL4 UAS-Foxn1* rough-eye phenotype. The loss-of-function mutations consisted of (pre-existing) P-element insertions, and fly strains carrying these insertions were crossed to *GMR-GAL4 UAS-Foxn1/SM1* flies so as to test each mutation under heterozygous conditions. A total of 17 insertion mutations were tested, and only 2 insertions—the 2 in *lilli* (*lilli^{00632}* and *lilli^{k05431}*)—were suppressors. As predicted by the deficiency mapping of the suppressor, *lilli* is located in region 23C1-3.

Aff4-mutant mice

Mice were maintained in microisolator cages under specific pathogen-free conditions in a 12-hr light/dark cycle. Males and females were analyzed in every experiment; no gender-based differences in results were observed or expected. Animal numbers were consistent with standards in the field. Institutional Animal Care and Use Committees approved all work with vertebrate animals reported here.

The *Aff4* mutant alleles generated in this study are shown in Fig EV3A. *Aff4^{neo}* was created by homologous recombination using the targeting construct pYK5-7 and the ES-cell line KV1, a 129-C57BL/6 hybrid line. pYK5-7 was constructed using recombineering reagents and protocols developed by Liu *et al* (2003) and available from the National Cancer Institute (NCI) at Frederick (see https://frederick.cancer.gov/Science/BrbRepository/Home#/recombineeringInformation). The targeting construct contained a 12-kb *Aff4* genomic fragment that extended from nucleotide 2,828 of intron 6 to nucleotide 43 of intron 13. This 12-kb fragment was derived from murine strain C57BL/6 and was retrieved from BAC RP24-395F7 using plasmid PL253 (BAC RP24-395F7 was obtained from the BACPAC Resources Center of the Children's Hospital Oakland Research Institute). To construct pYK5-7, a *loxP* site and *Sac* I site were inserted 183-bp upstream of exon 10 using plasmid PL452. A *loxP* site, *FRT*-flanked neomycin-resistance (*neo^R*) cassette, and *Eco*R I site were then inserted 321-bp downstream of exon 11 using plasmid PL451. Accordingly, the construct's 5′ (long) arm was 5.4 kb, the 3′ (short) arm was 3.8 kb, and the *loxP* sites were 2.8 kb apart. The plasmid's configuration was confirmed by sequencing prior to electroporation into KV1 cells.

Aff4^{neo} alleles were identified in 42 ES-cell clones by PCR-based screening for homologous recombination. Six of these clones were selected for Southern blotting and confirmed to possess correctly targeted *Aff4*. Two correctly targeted clones—1E4 and 2E7—were injected separately into blastocysts, and the resulting chimeric mice were bred to strain C57BL/6 (Charles River Laboratories) once so as to establish two independent lines of *Aff4*-mutant mice. These lines, also called 1E4 and 2E7, were subsequently confirmed by Southern blotting to possess correctly configured *Aff4^{neo}* alleles (see Southern blotting). The electroporation of KV1 cells, cultivation of ES-cell clones, and injection of blastocysts were performed at the Transgenic Mouse Shared Resource of the Herbert Irving Comprehensive Cancer Center (Columbia University Medical Center). The 1E4 and

2E7 murine lines were maintained separately, with members of a line bred to each other or to the transgenic lines described below. Mice that were $Aff4^{+/neo}$ or $Aff4^{neo/neo}$ appeared wild type, suggesting that $Aff4^{neo}$ was not significantly impaired in function by its insertion mutations.

$Aff4^{neo}$ was converted to $Aff4^{flox}$ in the germline by crossing the transgene *ACTB-FLPe* (strain background C57BL/6; The Jackson Laboratory) into the 1E4 and 2E7 lines and then crossing the progeny to C57BL/6. Mice that possessed the $Aff4^{flox}$ allele and lacked the *ACTB-FLPe* transgene were used to establish $Aff4^{flox}$ lines (1E4 or 2E7). $Aff4^{flox}$ was converted to $Aff4^{ko}$ in the germline by crossing the transgene *EIIa-cre* (strain background C57BL/6; The Jackson Laboratory) into the 1E4 and 2E7 lines and then crossing the progeny to C57BL/6. Mice that carried the $Aff4^{ko}$ allele and lacked the *EIIa-cre* transgene were used to establish $Aff4^{ko}$ lines (1E4 or 2E7). To generate *Aff4* conditional knockouts, the transgene *KRT14-cre* (strain background 129-C57BL/6 mixed) was crossed into the two $Aff4^{flox}$ lines. To generate $Aff4^{ko}$ $Foxn1^-$ or $Aff4^{flox}$ $Foxn1^-$ double mutants, the *Aff4* and *Foxn1* mutations were linked together on the same chromosome by spontaneous homologous recombination (the *Foxn1* and *Aff4* genes are 24.9 Mbp apart on chromosome 11). $Aff4^{+/ko}$ or $Aff4^{flox/flox}$ females were crossed to $Foxn1^{-/-}$ males (strain background 129-C57BL/6 mixed), the $Aff4^{+/ko}$ $Foxn1^{+/-}$ or $Aff4^{+/flox}$ $Foxn1^{+/-}$ female progeny were crossed to $Foxn1^{-/-}$ males, and the resulting $Aff4^{+/ko}$ $Foxn1^{-/-}$ or $Aff4^{+/flox}$ $Foxn1^{-/-}$ male recombinants were crossed to $Aff4^{+/ko}$ $Foxn1^{+/-}$ or $Aff4^{+/flox}$ $Foxn1^{+/-}$ females to generate double-mutant lines.

Mouse genotyping

Murine DNA was prepared by clipping a 1–2 mm segment of tail or toe, adding 400 µl of 50 mM NaOH, heating at 95°C for 30 min, vortexing, neutralizing with 40 µl of 1 M Tris–HCl (pH 8.0), and centrifuging at 20,817 ×g for 5 min to pellet debris. Each lysate was stored at −20°C, and 1 µl of supernatant was used for PCR. PCR was performed with GoTaq Green Master Mix (Promega) and the following primer pairs: (i) to detect $Aff4^{neo}$, 5′-TGACTGGGCACAACAGAC AATC and 5′-AGCCAACGCTATGTCCTGATAG; (ii) to detect/distinguish $Aff4^{flox}$ and $Aff4^+$, 5′-GACATTGTTACTAGTACTTAACTTTG and 5′-TTTCCAGTTATGCACTATAGTGTAC; (iii) to detect $Aff4^{ko}$, 5′-AGTTGTGATGGTGATTGTATCATTC and 5′-TTTCCAGTTATGCACT ATAGTGTAC; (iv) to detect *cre* transgenes, 5′-GGTCGATGCAACG AGTGATGAGGT and 5′-CAGCATTGCTGTCACTTGGTCGTG; (v) to detect $Foxn1^-$, 5′-TGCGTGACTACCTACGGGTAAC and 5′-GATCGA CAGATTTGATCCAGCG; (vi) to detect $Foxn1^+$, 5′-ATTATCTCAGTAC AGCACAGG and 5′-GAATTTGGTTGTGTTCCTGGC; (vii) to detect *ACTB-FLPe*, 5′-ATCACTGATATTGTAAGTAGTTTGC and 5′-TAGT GATCAGGTATTGCTGTTATC. The general PCR program was as follows: 97°C, 1 min 30 s ᐧ 96°C, 30 s/ 56–60°C, 30 s/72°C, 30 s [2 cycles] ᐧ 94°C, 30 s/ 56–60°C, 30 s/ 72°C, 30 s [28–33 cycles] ᐧ 72°C, 5 min ᐧ 4°C, hold. The precise annealing temperature used depended on the primers.

Antibody production

Rabbit polyclonal antibodies were generated against the following antigens: (i) murine FOXN1 amino acids (a.a.) 1–648 fused to glutathione S-transferase (GST), (ii) murine AFF4 a.a. 84–232 fused

to GST, or (iii) human AFF4 a.a. 1–750 tagged with polyhistidine (His). The resulting antibodies were named α-FOXN1 (FL), α-AFF4 (YK6), or α-AFF4^{750}, respectively (Baxter & Brissette, 2002; Niedzielski *et al*, 2007). The two GST-fusion proteins were produced using pGEX-2T (GE Healthcare Life Sciences), while the His-tagged protein was generated using pET-6HIS-11d (Novagen). All antigens were synthesized in *E. coli* according to expression-vector instructions, were purified using matrix-immobilized glutathione (to bind GST) or nickel (to bind the His-tag), and were isolated or analyzed on polyacrylamide gels prior to injection into rabbits. α-FOXN1 (FL) and α-AFF4 (YK6) were raised and affinity purified at Strategic BioSolutions/SDIX, while α-AFF4^{750} was raised at Covance.

Immunofluorescence

Tissue samples were embedded without fixation in O.C.T. compound (Tissue Tek) in Peel-A-Way trays (Polysciences) in a 2-methylbutane bath at −70°C. Sections (~6 µm) were fixed immediately after adherence to a slide (while wet) with 1:1 methanol:acetone (for AFF4 or FOXN1 staining) or 100% methanol (for DLL4 or KRT86 staining) at −20°C, air-dried, and stored at −80°C. To stain by indirect immunofluorescence, sections were placed in a humidified chamber, hydrated with 0.1% NP-40/PBS, blocked with SuperBlock T20 (PBS) Blocking Buffer (Thermo Fisher Scientific) at room temperature for 15 min, blocked using the Vector Laboratories Avidin/Biotin Blocking Kit, and then incubated with the primary antibody (or antibodies) in Superblock T20 (PBS) at 4°C overnight. The primary antibodies employed were as follows: FOXN1 (G-20; Santa Cruz Biotechnology), α-AFF4 (YK6), or α-AFF4^{750}, human/ mouse DLL4 antibody (rat monoclonal 207822; R&D Systems), or Keratin 86 (L-14; Santa Cruz Biotechnology). All remaining steps were performed at room temperature. Sections were washed 3 times with 0.1% NP-40/PBS (5 min per wash) and incubated with a biotinylated secondary antibody in Superblock T20 (PBS) for 1 h. Depending on the primary antibody to be visualized, the biotinylated secondary antibodies were horse anti-goat IgG (Vector Laboratories), horse anti-rabbit IgG (Vector Laboratories), or mouse anti-rat IgG (Jackson ImmunoResearch). Sections were washed 3 times with 0.1% NP-40/PBS (5 min per wash) and incubated with streptavidin-CY3 (Millipore Sigma) in Superblock T20 (PBS) for 1 hr. For red/green double staining, DyLight 488-conjugated goat anti-rabbit IgG antibody (Vector Laboratories) was added along with the streptavidin-CY3. Sections were then washed once with 0.1% NP-40/PBS (5 min), incubated with Hoechst 33258 (Millipore Sigma) at 1 µg/ ml in 0.1% NP-40/PBS (2 min), washed once with 0.1% NP-40/PBS (5 min), and washed briefly (dipped) in distilled H_2O. Most water was removed by careful aspiration, and the sections were air-dried and mounted with a glycerol-based mounting medium (KPL Fluorescent Mounting Media, SeraCare). Staining for thymic markers followed the same basic procedure but used antibodies purchased from Covance (IVL, KRT5), Developmental Studies Hybridoma Bank (KRT8), Santa Cruz Biotechnology (pan-keratin), eBioscience (CD11C, γδ TCR), or Invitrogen (B220, CD4, CD8, CD19).

Southern blotting

Southern blotting was performed with genomic DNA isolated from primary cultures of murine keratinocytes. Cultures were prepared

from trypsin-treated skins of newborn mice and grown to confluence at 34°C in minimal essential medium with 4% chelex-treated fetal calf serum, 50 μM $CaCl_2$, and 2.5 ng/ml epidermal growth factor. Genomic DNA was isolated using the Qiagen QIAamp DNA Mini Kit. For each murine line, 20 μg of DNA was digested with either *Sac* I or *Eco*R I, electrophoresed on a 0.7% agarose gel, denatured, neutralized, transferred to Hybond-N (GE Healthcare Life Sciences), and cross-linked with UV light. 5′-arm blots (*Sac* I-digested genomic DNA) were probed with DNA corresponding to nucleotides 2,525–2,682 of intron 6. 3′-arm blots (*Eco*R I-digested genomic DNA) were probed with DNA corresponding to nucleotides 363–544 of intron 13. Probes were made by PCR using BAC RP24-395F7 as the template. For 5′-arm blots, the PCR primer pair was 5′-CAAAGCTGTGCAATTATAATGCTG and 5′-TCTGGAGACAGGGTCT-TACTAC. For 3′-arm blots, the PCR primer pair was 5′-AATTTT-GAGGTAGAGTCTTACAATG and 5′-CAAATTTCAGTCTATAAACA CCAAG. Probes were labeled with ^{32}P using [α-^{32}P]-dCTP and Ready-To-Go DNA Labeling Beads (GE Healthcare Life Sciences). Blots were pre-hybridized and hybridized at 60°C in 250 mM Na_2HPO_4, 288 mM NaH_2PO_4 (pH 7.0), 1 mM EDTA-Na_2, 7% SDS, 1% bovine serum albumin (BSA), and 100 μg/ml fish sperm DNA (boiled and quenched on ice, either alone for pre-hybridization or with probe for hybridization). Blots were washed at 60°C in 0.1X SSC, 0.1% SDS, and visualized by autoradiography.

Assays for soluble FOXN1-AFF4 complexes

The ability of FOXN1 and AFF4 to form soluble complexes was assayed using 3 different cell-culture systems: (i) HEK-293 cells that produced full-length, FLAG-tagged murine FOXN1 (Prowse *et al*, 1999) and full-length, MYC-tagged human AFF4 from transiently transfected plasmids, (ii) wild-type, primary murine keratinocytes (*Foxn1*$^{+/+}$, *Aff4*$^{+/+}$), and (iii) wild-type, primary murine keratinocytes that produced full-length, FLAG-tagged murine FOXN1 from an adenoviral vector (Ad-Foxn1; Li *et al*, 2007). In all experiments, to detect FOXN1-AFF4 complexes, cellular constituents were extracted from cultures, immunoprecipitated using antibodies to one of the two proteins of interest (either FOXN1 or AFF4), and then immunoblotted using antibodies to the other protein (Calautti *et al*, 1998). Depending on the experiment, antibodies were anti-FOXN1, anti-AFF4, anti-FLAG (M2; Millipore Sigma), or anti-MYC tag (9E10; Santa Cruz Biotechnology). In transient transfection experiments, pcDNA3-based plasmids expressed either a FOXN1 or AFF4 cDNA and were co-transfected using Lipofectamine (Invitrogen). Empty vectors (plasmids or Ad virus without an inserted cDNA) were used as controls.

RNA analyses

For each RNA preparation, skin was isolated from the entire back of 1 mouse at age P6. The skin was washed briefly with cold PBS, the subcutaneous fat was peeled away with forceps, and the skin was cut in half. Mesenchyme was then largely removed via heat shock so as to enrich for epithelium (epidermis and hair follicles). In brief, the two skin pieces were plunged into a beaker of PBS at 60°C and incubated for 30 s. The skin pieces were then transferred to a beaker of cold PBS (on ice) and submerged for 1 min with slow, gentle stirring by hand (with forceps). The skin pieces were next transferred

to a dry petri dish, flattened with the dermal sides down, and grasped at the edges of the epithelial and dermal compartments with separate forceps. The epithelium and mesenchyme were peeled apart, and the epithelial tissue was snap-frozen using liquid nitrogen. The frozen tissue was ground to a powder using a pre-cooled mortar and pestle. RNA was then isolated from the powdered tissue using the RNeasy Mini Kit plus QIAshredder (Qiagen).

To eliminate contaminating DNA, the RNA preparations were treated with TURBO DNAse (2 units per 2 μg of RNA prep; Ambion/Invitrogen) at 37°C for 30 min. The DNAse was then inactivated using EDTA-Na_2 (added to a final concentration of 15 mM) and heat (65°C for 10 min). A 1/10th volume of 0.3 M sodium acetate was added, and the RNA was ethanol precipitated, dried, and resuspended in RNAse-free water.

RNA-seq libraries were prepared using DNAse-treated RNA (1 μg per library) and the Illumina TruSeq Stranded Total RNA Ribo-Zero H/M/R Gold Kit. Each library underwent ribosomal depletion according to the kit's instructions, was constructed using indexed adapters, was quantified using the KAPA Complete Library Quantification Kit, and was confirmed for quality using an Agilent 2200 TapeStation.

Gene expression analyses compared phenotypically mutant animals to closely related, phenotypically wild-type animals. Accordingly, *Aff4*-cko (*KRT14-cre; Aff4*$^{flox/flox}$) mice were compared to *KRT14-cre; Aff4*$^{+/flox}$ mice, and *Foxn1*-null (*Foxn1*$^{nu/nu}$; Taconic Biosciences) mice were compared to *Foxn1*$^{+/nu}$ mice. Three libraries were prepared for each genotype, and each library was derived from a different mouse/RNA preparation. Hence, a total of 12 indexed libraries were prepared.

The 12 indexed libraries were pooled and sequenced using 2 lanes of an Illumina HiSeq 2500, V4 chemistry, and 50-bp paired-end reads. Raw sequencing data were received in FASTQ format. Read mapping used Tophat 2.0.9 against the mm10 mouse reference genome. The resulting BAM alignment files were processed with the HTSeq 0.6.1 python framework and respective mm10 GTF gene annotation (UCSC database). The Bioconductor package DESeq2 (3.2) was used to identify differentially expressed genes (DEG) and for statistical analysis based on the negative binomial distribution model. The resulting values were adjusted using the Benjamini–Hochberg method for false discovery rate. Genes with an adjusted *P*-value < 0.05 were determined to be differentially expressed. Library quality control, sequencing, and data analyses were performed at the Genome Technology Center of New York University Medical Center.

Krt86 pre-mRNA levels were measured by real-time RT–PCR. DNAse-treated RNA (2 μg of each prep) was reverse transcribed into cDNA using the Verso cDNA Synthesis Kit (Thermo Fisher Scientific) and random primers (42°C, 30 min synthesis). cDNA preparations were serially diluted and analyzed using a Bio-Rad iCycler-MyiQ system and IQ SYBR Green Supermix. PCR results were judged valid only if product levels/cycle numbers changed in step with the dilutions of the cDNA samples. The following primer pairs were used to assay the 5′, mid, and 3′ sites of the *Krt86* pre-mRNA (locations relative to the transcription start site appear in parentheses): (i) 5′-GAGAAGGAGCAGATCAAGTGTC and 5′-TGAGACTAGA GGCTCAATATGAG (+389 to +551) (ii) 5′-TCAAGGCTCAGTATGAT-GACATTG and 5′-CAAGAAGCCCTTTCCAATAGATTC (+3,083 to +3,224; mid), and (iii) 5′-CTGCGGAGACTCTTGGCAATG and

5′-CGCTGCACACTCTTGTGTTGAC (+5,837 to +5,985; 3′). Results were normalized by comparing *Hprt* expression, which was measured in each sample using the primer pair 5′-ACCTCTCGAAGTGTTGGATACAG and 5′-TTCACTAATGACA-CAAACGTGATTC. The general real-time PCR program was as follows: 95°C, 3 min ◦ 96°C, 30 s/ 57–58°C, 30 s/ 72°C, 30 s [2 cycles] ◦ 94°C, 30 s/ 57–58°C, 30 s/ 72°C, 30 s [38 cycles] ◦ Melting curve cycle (95°C, 1 min ◦ 55°C, 1 min, increment 0.5°C). The precise annealing temperature used depended on the primers. Results were analyzed statistically using two-way ANOVA with post hoc Sidak's multiple comparison test at a 95% confidence interval.

The following primers were used to assay the expression of thymic markers: *Aire*, 5′-CCTCTTGGAAACGGAATTCAGAC and 5′-CTGAATGCACTTCTTGGATCTTC; *Ccl25*, 5′-AGAGGGCGATGAGA ATCTTGAC and 5′-GGCACTCCTCACGCTTGTACTG; *Cdr1*, 5′-CGGT GGATTTTCAGGAAGACATG and 5′-TAATGTCTTCCTGAAGATTGA-CATC; *Cldn3*, 5′-GTCAGATGCAGTGCAAAATGTAC and 5′-GTCTTG TACGCAGTTGGTACAC; *Cldn4*, 5′-CCCTTATGGTCATCAGCAT-CATC and 5′-GGCACCATAATCAGCATGCTTG; *Cxcl12*, 5′-TTTCG GGTCAATGCACACTTGTC and 5′-ATCAGTGACGGTAAACCAGTC AG; *Dsc3*, 5′-AACAGACCCAGTGACAAATGAAG and 5′-CCTTCA-CATGTACTGTAACCATAG; *Ivl*, 5′-CTGTGAGTTTGTTTGGTCTAC AG and 5′-AGACCTGGCATTGTGTAGGATG; *Lekt1*, 5′-ATGAATGT-GAAGGTTTTGTCAAGAG and 5′-AGTGTCAGATGGACAGATGAAA TC; *Lgals7*, 5′-GGCTGGCAGGTTCCATGTAAAC and 5′-TGGAAGTG-GAGATATTCGTCATC; *Lhx2*, 5′-GCCAAGGACTTGAAGCAGCTTG and 5′-AGCGTGGCATCTGACGTCTTG; *Ly51*, 5′-TGCATCGGTT-CACTGCTATAGAG and 5′-TGGAATAGCAATTTTATCCAGTTTAG; *Ocln*, 5′-AAGGTGTCTCTAGGTTACCATTG and 5′-GACTATGCG-GAAAGAGTTGACAG; *Psmb11*, 5′-ACCCACCGTGATGCTTATTCAG and 5′-AGGCTCAGGATAGTTCCACAAG.

Chromatin immunoprecipitation (ChIP) assays of intact tissue

For each ChIP assay, skin was harvested from 3 mice at age P7; each harvested sample consisted of the entire back skin. After each skin was taken, it was washed briefly with cold PBS, and the subcutaneous fat was peeled away with forceps. The skin was next cut into strips (2–3 mm wide), and each strip was placed immediately (as it was cut) into 4% formaldehyde in PBS (10 ml per skin). Strips were shaken in the formaldehyde solution for 15 min at room temperature, washed briefly with PBS, removed from the PBS, snap-frozen in liquid nitrogen, and stored at −80°C.

To isolate fixed chromatin, skin strips were ground into a fine powder in liquid nitrogen using a pre-cooled mortar and pestle. Subsequent steps of the protocol were a modified version of the procedures described in Hu *et al* (2016). Powdered skin was placed in lysis buffer 1 (10 ml per skin; 30 ml total per ChIP), which consisted of 50 mM HEPES-KOH (pH 7.5), 140 mM NaCl, 1 mM EDTA-Na₂, 10% glycerol, 0.5% NP-40, and 0.25% Triton X-100. Samples were rocked at 4°C for 1 h and then centrifuged at 3,488 ×*g* at 4°C for 5 min. Supernatants were discarded, and fat aggregates on tube walls were removed with Kimwipes. Pellets were resuspended in a solution of 200 mM NaCl, 10 mM Tris–HCl (pH 8.0), 1 mM EDTA-Na₂, and 0.5 mM EGTA at a volume of 10 ml per skin. Suspensions were rocked for 25 min at 4°C and centrifuged at 1,083 ×*g* at 4°C for 5 min. Supernatants were discarded, and pellets were resuspended in lysis buffer 2—100 mM NaCl, 10 mM Tris–HCl (pH

8.0), 1 mM EDTA-Na₂, 0.5 mM EGTA, 0.5% sarkosyl, 0.1% sodium deoxycholate, and 0.2% SDS (SDS was added freshly)—at a volume of 10 ml per skin. Suspensions were rocked for 1 h at 4°C.

Samples were next sonicated so as to produce DNA fragments of 300–600 bp. Sonications were performed using a Bioruptor (Diagenode), and suspensions were sonicated in 1-ml aliquots in 15-ml polystyrene conical tubes. Upon the completion of sonication, the aliquots of each lysate were recombined, a 300 μl sample of each lysate was removed to assess the extent of DNA shearing (a shearing sample), and the remainder of each lysate was frozen at −80°C.

To analyze DNA fragmentation, shearing samples were centrifuged at 20,817 ×*g* for 10 min at 4°C, and supernatants (200 μl) were transferred to fresh tubes. NaCl was added to a final concentration of 0.3 M (20 μl of 3 M NaCl), and cross-links were reversed by heating samples overnight at 65°C. RNase A was added to a final concentration of 0.2 μg/μl, and samples were incubated for 1 h at 37°C. Proteinase K was then added to a final concentration of 0.2 μg/μl, and samples were incubated for 2 h at 56°C. Samples were extracted with 1 volume of phenol:chloroform:isoamyl alcohol (25:24:1), supernatants were transferred to fresh tubes, and glycogen (50 μg) was added to each supernatant. DNA was precipitated with 2 volumes of cold ethanol (−20°C), washed once with 70% ethanol, dried, and resuspended in 20 μl of TE (10 mM Tris–HCl pH 8.0, 1 mM EDTA-Na₂). The extent of fragmentation was then determined by electrophoresis of the DNA on 2% agarose gels.

Properly fragmented lysates were thawed and centrifuged at 1,560 ×*g* for 15 min at 4°C. Each supernatant was filtered through a cotton gauze pad (Fisherbrand Gauze Sponges, 12-ply, 3 × 3 in.) to remove debris.

Each ChIP used 20 ml of lysate. To set up a ChIP, lysate (20 ml) was transferred to a fresh tube (50-ml conical) and mixed with an equal volume (20 ml) of lysis buffer 2 minus SDS so as to dilute the SDS in the lysate to 0.1%. Each ChIP then received 1/10th volume of 10% Triton X-100 (final concentration, 1%) and 1/20th volume of 10% NP-40 (final concentration, 0.5%). An aliquot (50 μl) was removed from each ChIP and stored at −20°C as an input sample (used for the later measurement of input DNA).

Antibodies were added to ChIPs as pre-formed complexes in which the primary antibody was bound to a secondary antibody, and the secondary antibody was bound to protein G-coupled magnetic Dynabeads (Invitrogen). To generate these antibody-coupled beads, protein G-coupled Dynabeads (50 μl per ChIP) were washed 3 times with cold, freshly prepared 0.5% BSA in PBS (1.3 ml wash solution per 100 μl of beads). After the first wash, beads were pelleted by centrifugation at 956 ×*g* for 3 min at 4°C. In subsequent washes and other steps (couplings, precipitations), beads were pelleted using a magnetic stand unless otherwise specified.

The washed beads were mixed with secondary antibodies (12 μg per ChIP) in 0.5% BSA/PBS (650 μl per ChIP), and the mixtures were incubated with rotation overnight at 4°C. The secondary antibody-bead complexes were washed 5 times with cold 0.5% BSA/PBS (pelleted before and after each wash) and next incubated with primary antibodies in 0.5% BSA/PBS with rotation overnight at 4°C. The antibody-coupled beads were then washed 5 times with cold 0.5% BSA/PBS and resuspended in 100 μl of cold 0.5% BSA/PBS per IP.

Antibody-coupled beads (100 μl) were added to each ChIP, and the ChIPs were rotated overnight at 4°C. Beads were pelleted, and

supernatants were removed. The beads of each ChIP were next resuspended in 650 µl of cold RIPA buffer—500 mM NaCl, 50 mM Tris–HCl (pH 8.0), 1 mM EDTA-Na$_2$, 1% NP-40, 0.5% sodium deoxycholate, and 0.1% SDS—and transferred to a 1.5-ml tube. Using the same pipette tip, fresh RIPA buffer (650 µl) was added to the 50-ml tube in which the ChIP was performed and from which beads were just collected. The residual beads were collected and added to the previously collected beads (total RIPA volume now 1.3 ml per ChIP). The beads were pelleted again, washed 4 more times with cold RIPA buffer (1.3 ml), and washed once with a cold solution (1.3 ml) of 50 mM NaCl, 10 mM Tris–HCl (pH 8.0), and 1 mM EDTA-Na$_2$. Beads were then pelleted by centrifugation at 956 ×*g* for 3 min at 4°C, and supernatants were removed completely.

Chromatin was eluted from the beads through the addition of elution buffer (100 µl)—50 mM Tris–HCl (pH 8.0), 10 mM EDTA-Na$_2$, and 1% SDS—and incubation of the suspension at 65°C for 15 min, with brief vortexing performed every 3–4 min. Beads were then pelleted by centrifugation at 20,817 ×*g* for 1 min. The elutions (supernatants) were collected and transferred to fresh tubes. Fresh elution buffer (100 µl) was added to the beads of each ChIP, and the elution steps were repeated. The second elution was combined with the first for total eluted volumes of 200 µl per ChIP.

Input samples were thawed, and each was brought to a volume of 200 µl with elution buffer. All samples—input and ChIP—were then processed in the same way as the shearing samples (see above). Specifically, cross-links were reversed at 65°C in the presence of 0.3 M NaCl, digestions were performed with RNase A and proteinase K, and DNA was extracted with phenol:chloroform:isoamyl alcohol and then precipitated with ethanol. Dried DNA pellets were resuspended in 50 µl of 0.1X TE. As double-stranded DNA was not required for subsequent steps, the DNA solutions were boiled for 10 min to facilitate DNA resuspension and to eliminate remaining cross-links.

ChIP assay outcomes were determined by real-time PCR. PCRs were performed using the Bio-Rad iCycler-MyiQ system, IQ SYBR Green Supermix, and serial dilutions of the input or ChIPped DNA samples. PCR results were judged valid only if product levels/cycle numbers changed in step with the dilutions of the DNA samples. Assay results were normalized for input DNA and then compared. In each experiment, phenotypically mutant animals were compared to closely related, phenotypically wild-type animals; as such, *Aff4*-cko mice were compared to *Aff4$^{flox/flox}$* mice, and *Foxn1*-null (*Foxn1$^{nu/nu}$*) mice were compared to *Foxn1$^{+/nu}$* mice. A total of 25 genomic sites were assayed for the binding of AFF4 and FOXN1. Assayed sites were immediately upstream of the *Krt86* core promoter, were non-coding regions conserved in other mammals, and/or contained consensus-binding sequences for FOXN1. The ChIP sites shown in Fig 7 were assayed using the following PCR primers (locations relative to the mRNA start site appear in parentheses): (i) 5′-GGGATC-CATAACTCTGCATTTTG and 5′-TTCACTTGGTCTTAGAAGAGAATC (−2,195 to −2,123), (ii) 5′-GTTTGTGAGGACATCTTTCCTTAG and 5′-GGAACACCATTATTCTACTGAATG (−2,025 to −1,892), and (iii) 5′-ACTCCTACTACTCTTTCAAGATATG and 5′-TTGGGGATATGTT-GACAGCTTTG (−1,823 to −1,721). The ChIP sites shown in Fig 8 were assayed using the following PCR primers (locations appear in parentheses): (i) 5′-ATAAAGCCATCTAATTGCTTCAGAC and 5′-GGGAGAAGGGCAACTCTGAAAC (−86 to +64), (ii) 5′-ATGCT-CAGTGTGTGAAGCATGAG and 5′-TGTGACATGCTGTGCTCCGGG

(+366 to +487), (iii) 5′-AGAGAAGAGTTTAGGACACGATG and 5′-TCTACAGACTACTCGATGTACTTC (+2,676 to +2,823), (iv) 5′-AGGAAATCTGTGTAAGTCCTTTAAC and 5′-GGTGGAGCCTAAG-TATGAGTAC (+4,111 to +4,280), and (v) 5′-AACACTT-GAGCTTGCTGCGGAG and 5′-ACGCAGAGATCGCCACAGACG (+5,823 to +5,944). ChIP assays of the *Krt86* TSS for the binding of FOXN1 or AFF4 used the following PCR primers: 5′-CTAAAGAGG-TAAACACTGAATTCAC and 5′-GATCCGCAAGTCATGGTTATTTAG (−14 to +87). The ChIP assays used the same general real-time PCR program as the RNA analyses. Assay results were analyzed statistically using one-way ANOVA with post hoc Tukey's multiple comparison test at a 95% confidence interval.

The primary antibodies used in specific ChIP assays were as follows: (i) for AFF4 ChIPs—α-AFF4 (YK6), 6 µg per ChIP; (ii) for FOXN1 ChIPs—a mixture of FOXN1 (G-20) and α-FOXN1 (FL), 700 ng and 4 µg, respectively, per ChIP; (iii) for total Pol II—monoclonal 8WG16, 10 µg per ChIP; (iv) for P-Ser5 Pol II—monoclonal H14, 10 µg per ChIP; (v) for P-Ser2 Pol II—monoclonal H5, 10 µg per ChIP. The 3 monoclonal antibodies to Pol II were from Covance/BioLegend.

All secondary antibodies were from Vector Laboratories (unconjugated). The secondary antibodies used in specific ChIP assays were as follows: (i) for AFF4 ChIPs—goat anti-rabbit IgG; (ii) for FOXN1 ChIPs—a mixture of rabbit anti-goat IgG (6 µg bound to 25 µl of beads/ChIP) and goat anti-rabbit IgG (6 µg bound to a separate 25 µl of beads/ChIP); (iii) for total Pol II ChIPs—goat anti-mouse IgG; (iv) for P-Ser5 Pol II ChIPs and P-Ser2 Pol II ChIPs—goat anti-mouse IgM.

Statistical analyses

Statistical methods used in RNA-seq DEG identification, *Krt86* pre-mRNA measurements, or ChIP assays are described in the two preceding sections, "RNA Analyses" or "Chromatin Immunoprecipitation (ChIP) Assays of Intact Tissue". Statistical analyses of the pre-mRNA or ChIP experimental results were performed using GraphPad Prism 7; numerical calculations, error bars, denotations of significance, and sample sizes are explained in the figure legends.

Data availability

Datasets EV1 and EV2 present the primary (processed) data generated in the RNA-seq-based analysis of differential gene expression. The raw and processed RNA-seq data have been deposited in the Gene Expression Omnibus, accession # GSE152247 (see https://www.ncbi.nlm.nih.gov/geo/query/acc.cgi?acc = GSE152247).

Expanded View for this article is available online.

References

Abitbol M, Bosse P, Thomas A, Tiret L (2015) A deletion in FOXN1 is associated with a syndrome characterized by congenital hypotrichosis and short life expectancy in Birman cats. *PLoS One* 10: e0120668

Alfonso-Dunn R, Turner AW, Jean Beltran PM, Arbuckle JH, Budayeva HG, Cristea IM, Kristie TM (2017) Transcriptional elongation of hsv immediate early genes by the super elongation complex drives lytic infection and reactivation from latency. *Cell Host Microbe* 21: 507–517.e5

Bajoghli B, Aghaallaei N, Hess I, Rode I, Netuschil N, Tay BH, Venkatesh B, Yu JK, Kaltenbach SL, Holland ND *et al* (2009) Evolution of genetic networks underlying the emergence of thymopoiesis in vertebrates. *Cell* 138: 186–197

Baxter RM, Brissette JL (2002) Role of the nude gene in epithelial terminal differentiation. *J Invest Dermatol* 118: 303–309

Bentley DL (2014) Coupling mRNA processing with transcription in time and space. *Nat Rev Genet* 15: 163–175

Biggin MD (2011) Animal transcription networks as highly connected, quantitative continua. *Dev Cell* 21: 611–626

Blackburn CC, Augustine CL, Li R, Harvey RP, Malin MA, Boyd RL, Miller JF, Morahan G (1996) The nu gene acts cell-autonomously and is required for differentiation of thymic epithelial progenitors. *Proc Natl Acad Sci USA* 93: 5742–5746

Brand AH, Manoukian AS, Perrimon N (1994) Ectopic expression in *Drosophila*. *Methods Cell Biol* 44: 635–654

Brand AH, Perrimon N (1993) Targeted gene expression as a means of altering cell fates and generating dominant phenotypes. *Development* 118: 401–415

Bredenkamp N, Nowell CS, Blackburn CC (2014a) Regeneration of the aged thymus by a single transcription factor. *Development* 141: 1627–1637

Bredenkamp N, Ulyanchenko S, O'Neill KE, Manley NR, Vaidya HJ, Blackburn CC (2014b) An organized and functional thymus generated from FOXN1-reprogrammed fibroblasts. *Nat Cell Biol* 16: 902–908

Brissette JL, Li J, Kamimura J, Lee D, Dotto GP (1996) The product of the mouse nude locus, Whn, regulates the balance between epithelial cell growth and differentiation. *Genes Dev* 10: 2212–2221

Calautti E, Cabodi S, Stein PL, Hatzfeld M, Kedersha N, Dotto GP (1998) Tyrosine phosphorylation and src family kinases control keratinocyte cell-cell adhesion. *J Cell Biol* 141: 1449–1465

Cheah PY, Chia W, Yang X (2000) Jumeaux, a novel *Drosophila* winged-helix family protein, is required for generating asymmetric sibling neuronal cell fates. *Development* 127: 3325–3335

Chen FX, Smith ER, Shilatifard A (2018) Born to run: control of transcription elongation by RNA polymerase II. *Nat Rev Mol Cell Biol* 19: 464–478

Chen L, Xiao S, Manley NR (2009) Foxn1 is required to maintain the postnatal thymic microenvironment in a dosage-sensitive manner. *Blood* 113: 567–574

Chen Y, Cramer P (2019) Structure of the super-elongation complex subunit AFF4 C-terminal homology domain reveals requirements for AFF homo- and heterodimerization. *J Biol Chem* 294: 10663–10673

Cheng L, Guo J, Sun L, Fu J, Barnes PF, Metzger D, Chambon P, Oshima RG, Amagai T, Su DM (2010) Postnatal tissue-specific disruption of transcription factor FoxN1 triggers acute thymic atrophy. *J Biol Chem* 285: 5836–5847

Core L, Adelman K (2019) Promoter-proximal pausing of RNA polymerase II: a nexus of gene regulation. *Genes Dev* 33: 960–982

Dahl NA, Danis E, Balakrishnan I, Wang D, Pierce A, Walker FM, Gilani A, Serkova NJ, Madhavan K, Fosmire S *et al* (2020) Super elongation complex as a targetable dependency in diffuse midline glioma. *Cell Rep* 31: 107485

de Nooij JC, Hariharan IK (1995) Uncoupling cell fate determination from patterned cell division in the *Drosophila* eye. *Science* 270: 983–985

Estable MC, Naghavi MH, Kato H, Xiao H, Qin J, Vahlne A, Roeder RG (2002) MCEF, the newest member of the AF4 family of transcription factors involved in leukemia, is a positive transcription elongation factor-b-associated protein. *J Biomed Sci* 9: 234–245

Francisco JC, Dai Q, Luo Z, Wang Y, Chong RH, Tan YJ, Xie W, Lee GH, Lin C (2017) Transcriptional elongation control of hepatitis B virus covalently closed circular DNA transcription by super elongation complex and BRD4. *Mol Cell Biol* 37: e00040-17

Frank J, Pignata C, Panteleyev AA, Prowse DM, Baden H, Weiner L, Gaetaniello L, Ahmad W, Pozzi N, Cserhalmi-Friedman PB *et al* (1999) Exposing the human nude phenotype. *Nature* 398: 473–474

Frazer KA, Pachter L, Poliakov A, Rubin EM, Dubchak I (2004) VISTA: computational tools for comparative genomics. *Nucleic Acids Res* 32: W273–279

Freeman M (1996) Reiterative use of the EGF receptor triggers differentiation of all cell types in the *Drosophila* eye. *Cell* 87: 651–660

Galbraith MD, Allen MA, Bensard CL, Wang X, Schwinn MK, Qin B, Long HW, Daniels DL, Hahn WC, Dowell RD *et al* (2013) HIF1A employs CDK8-mediator to stimulate RNAPII elongation in response to hypoxia. *Cell* 153: 1327–1339

Gardini A, Baillat D, Cesaroni M, Hu D, Marinis JM, Wagner EJ, Lazar MA, Shilatifard A, Shiekhattar R (2014) Integrator regulates transcriptional initiation and pause release following activation. *Mol Cell* 56: 128–139

Gould SJ (1997) The exaptive excellence of spandrels as a term and prototype. *Proc Natl Acad Sci USA* 94: 10750–10755

Gould SJ, Lewontin RC (1979) The spandrels of San Marco and the Panglossian paradigm: a critique of the adaptationist programme. *Proc R Soc Lond B Biol Sci* 205: 581–598

Graur D, Li W-H (2000) *Fundamentals of molecular evolution*, 2nd edn. Sunderland, MA: Sinauer

Gu Y, Nelson DL (2003) FMR2 function: insight from a mouse knockout model. *Cytogenet Genome Res* 100: 129–139

Hardison RC, Taylor J (2012) Genomic approaches towards finding cis-regulatory modules in animals. *Nat Rev Genet* 13: 469–483

Hazelett DJ, Bourouis M, Walldorf U, Treisman JE (1998) decapentaplegic and wingless are regulated by eyes absent and eyegone and interact to direct the pattern of retinal differentiation in the eye disc. *Development* 125: 3741–3751

He N, Liu M, Hsu J, Xue Y, Chou S, Burlingame A, Krogan NJ, Alber T, Zhou Q (2010) HIV-1 Tat and host AFF4 recruit two transcription elongation factors into a bifunctional complex for coordinated activation of HIV-1 transcription. *Mol Cell* 38: 428–438

He S, Zhang G, Wang J, Gao Y, Sun R, Cao Z, Chen Z, Zheng X, Yuan J, Luo Y *et al* (2019) 6mA-DNA-binding factor Jumu controls maternal-to-zygotic transition upstream of Zelda. *Nat Commun* 10: 2219

Hofmann A, Brunner M, Schwendemann A, Strodicke M, Karberg S, Klebes A, Saumweber H, Korge G (2010) The winged-helix transcription factor JUMU regulates development, nucleolus morphology and function, and chromatin organization of *Drosophila melanogaster*. *Chromosome Res* 18: 307–324

Hozumi K, Mailhos C, Negishi N, Hirano K, Yahata T, Ando K, Zuklys S, Hollander GA, Shima DT, Habu S (2008) Delta-like 4 is indispensable in thymic environment specific for T cell development. *J Exp Med* 205: 2507–2513

Hu Y, Zhang Z, Kashiwagi M, Yoshida T, Joshi I, Jena N, Somasundaram R, Emmanuel AO, Sigvardsson M, Fitamant J *et al* (2016) Superenhancer reprogramming drives a B-cell-epithelial transition and high-risk leukemia. *Genes Dev* 30: 1971–1990

Jeronimo C, Collin P, Robert F (2016) The RNA polymerase II CTD: the increasing complexity of a low-complexity protein domain. *J Mol Biol* 428: 2607–2622

Jonkers I, Lis JT (2015) Getting up to speed with transcription elongation by RNA polymerase II. *Nat Rev Mol Cell Biol* 16: 167–177

Khersonsky O, Tawfik DS (2010) Enzyme promiscuity: a mechanistic and evolutionary perspective. *Annu Rev Biochem* 79: 471–505

Kirschner N, Brandner JM (2012) Barriers and more: functions of tight junction proteins in the skin. *Ann N Y Acad Sci* 1257: 158–166

Koch U, Fiorini E, Benedito R, Besseyrias V, Schuster-Gossler K, Pierres M, Manley NR, Duarte A, Macdonald HR, Radtke F (2008) Delta-like 4 is the essential, nonredundant ligand for Notch1 during thymic T cell lineage commitment. *J Exp Med* 205: 2515–2523

Kohoutek J, Li Q, Blazek D, Luo Z, Jiang H, Peterlin BM (2009) Cyclin T2 is essential for mouse embryogenesis. *Mol Cell Biol* 29: 3280–3285

Kojima A, Saito M, Hioki K, Shimanura K, Habu S (1984) NFS/N-nu/ + mice can macroscopically be distinguished from NFS/N- +/+ littermates by their thymic size and shape. *Exp Cell Biol* 52: 107–110

Landry CR, Levy ED, Michnick SW (2009) Weak functional constraints on phosphoproteomes. *Trends Genet* 25: 193–197

Li J, Baxter RM, Weiner L, Goetinck PF, Calautti E, Brissette JL (2007) Foxn1 promotes keratinocyte differentiation by regulating the activity of protein kinase C. *Differentiation* 75: 694–701

Li M, Chiba H, Warot X, Messaddeq N, Gerard C, Chambon P, Metzger D (2001) RXR-alpha ablation in skin keratinocytes results in alopecia and epidermal alterations. *Development* 128: 675–688

Liang K, Smith ER, Aoi Y, Stoltz KL, Katagi H, Woodfin AR, Rendleman EJ, Marshall SA, Murray DC, Wang L *et al* (2018) Targeting processive transcription elongation via SEC disruption for MYC-induced cancer therapy. *Cell* 175: 766–779.e17

Liao CP, Booker RC, Morrison SJ, Le LQ (2017) Identification of hair shaft progenitors that create a niche for hair pigmentation. *Genes Dev* 31: 744–756

Lin C, Garrett AS, De Kumar B, Smith ER, Gogol M, Seidel C, Krumlauf R, Shilatifard A (2011) Dynamic transcriptional events in embryonic stem cells mediated by the super elongation complex (SEC). *Genes Dev* 25: 1486–1498

Lin C, Smith ER, Takahashi H, Lai KC, Martin-Brown S, Florens L, Washburn MP, Conaway JW, Conaway RC, Shilatifard A (2010) AFF4, a component of the ELL/P-TEFb elongation complex and a shared subunit of MLL chimeras, can link transcription elongation to leukemia. *Mol Cell* 37: 429–437

Liu P, Jenkins NA, Copeland NG (2003) A highly efficient recombineering-based method for generating conditional knockout mutations. *Genome Res* 13: 476–484

Luo Z, Lin C, Guest E, Garrett AS, Mohaghegh N, Swanson S, Marshall S, Florens L, Washburn MP, Shilatifard A (2012) The super elongation complex family of RNA polymerase II elongation factors: gene target specificity and transcriptional output. *Mol Cell Biol* 32: 2608–2617

Mandinova A, Kolev V, Neel V, Hu B, Stonely W, Lieb J, Wu X, Colli C, Han R, Pazin MJ *et al* (2009) A positive FGFR3/FOXN1 feedback loop underlies benign skin keratosis versus squamous cell carcinoma formation in humans. *J Clin Invest* 119: 3127–3137

McGurk L, Berson A, Bonini NM (2015) *Drosophila* as an *in vivo* model for human neurodegenerative disease. *Genetics* 201: 377–402

McNeill H (2010) Planar cell polarity: keeping hairs straight is not so simple. *Cold Spring Harb Perspect Biol* 2: a003376

Mecklenburg L, Tychsen B, Paus R (2005) Learning from nudity: lessons from the nude phenotype. *Exp Dermatol* 14: 797–810

Memczak S, Jens M, Elefsinioti A, Torti F, Krueger J, Rybak A, Maier L, Mackowiak SD, Gregersen LH, Munschauer M *et al* (2013) Circular RNAs are a large class of animal RNAs with regulatory potency. *Nature* 495: 333–338

Mi B, Xiong Y, Chen L, Yan C, Endo Y, Liu Y, Liu J, Hu L, Hu Y, Sun Y *et al* (2019) CircRNA AFF4 promotes osteoblast cells proliferation and inhibits apoptosis via the Mir-7223-5p/PIK3R1 axis. *Aging* 11: 11988–12001

Mueller D, Bach C, Zeisig D, Garcia-Cuellar MP, Monroe S, Sreekumar A, Zhou R, Nesvizhskii A, Chinnaiyan A, Hess JL *et al* (2007) A role for the MLL fusion partner ENL in transcriptional elongation and chromatin modification. *Blood* 110: 4445–4454

Mueller D, Garcia-Cuellar MP, Bach C, Buhl S, Maethner E, Slany RK (2009) Misguided transcriptional elongation causes mixed lineage leukemia. *PLoS Biol* 7: e1000249

Nakai Y, Nakajima K, Robert J, Yaoita Y (2016) Ouro proteins are not essential to tail regression during Xenopus tropicalis metamorphosis. *Genes Cells* 21: 275–286

Nehls M, Kyewski B, Messerle M, Waldschutz R, Schüddekopf K, Smith AJ, Boehm T (1996) Two genetically separable steps in the differentiation of thymic epithelium. *Science* 272: 886–889

Nehls M, Pfeifer D, Schorpp M, Hedrich H, Boehm T (1994) New member of the winged-helix protein family disrupted in mouse and rat nude mutations. *Nature* 372: 103–107

Niedzielski MF, Hopewell R, Ismail Z, Estable MC (2007) MCEF is localized to the nucleus by protein sequences encoded within three distinct exons, where it represses HIV-1 Tat-transactivation of LTR-directed transcription. *Int J Biol Sci* 3: 225–236

Niessen MT, Iden S, Niessen CM (2012) The *in vivo* function of mammalian cell and tissue polarity regulators–how to shape and maintain the epidermal barrier. *J Cell Sci* 125: 3501–3510

Nilson I, Reichel M, Ennas MG, Greim R, Knorr C, Siegler G, Greil J, Fey GH, Marschalek R (1997) Exon/intron structure of the human AF-4 gene, a member of the AF-4/LAF-4/FMR-2 gene family coding for a nuclear protein with structural alterations in acute leukaemia. *Br J Haematol* 98: 157–169

Nowell CS, Bredenkamp N, Tetelin S, Jin X, Tischner C, Vaidya H, Sheridan JM, Stenhouse FH, Heussen R, Smith AJ et al (2011) Foxn1 regulates lineage progression in cortical and medullary thymic epithelial cells but is dispensable for medullary sublineage divergence. *PLoS Genet* 7: e1002348

Okuda H, Kanai A, Ito S, Matsui H, Yokoyama A (2015) AF4 uses the SL1 components of RNAP1 machinery to initiate MLL fusion- and AEP-dependent transcription. *Nat Commun* 6: 8869

Okuda H, Takahashi S, Takaori-Kondo A, Yokoyama A (2016) TBP loading by AF4 through SL1 is the major rate-limiting step in MLL fusion-dependent transcription. *Cell Cycle* 15: 2712–2722

Prowse DM, Lee D, Weiner L, Jiang N, Magro CM, Baden HP, Brissette JL (1999) Ectopic expression of the nude gene induces hyperproliferation and defects in differentiation: implications for the self-renewal of cutaneous epithelia. *Dev Biol* 212: 54–67

Reissmann M, Ludwig A (2013) Pleiotropic effects of coat colour-associated mutations in humans, mice and other mammals. *Semin Cell Dev Biol* 24: 576–586

Rota IA, Dhalla F (2017) FOXN1 deficient nude severe combined immunodeficiency. *Orphanet J Rare Dis* 12: 6

Rybak-Wolf A, Stottmeister C, Glazar P, Jens M, Pino N, Giusti S, Hanan M, Behm M, Bartok O, Ashwal-Fluss R et al (2015) Circular RNAs in the mammalian brain are highly abundant, conserved, and dynamically expressed. *Mol Cell* 58: 870–885

Schlake T, Schorpp M, Maul-Pavicic A, Malashenko AM, Boehm T (2000) Forkhead/winged-helix transcription factor Whn regulates hair keratin gene expression: molecular analysis of the nude skin phenotype. *Dev Dyn* 217: 368–376

Schlake T, Schorpp M, Nehls M, Boehm T (1997) The *nude* gene encodes a sequence-specific DNA binding protein with homologs in organisms that lack an anticipatory immune system. *Proc Natl Acad Sci USA* 94: 3842–3847

Schorpp M, Schlake T, Kreamalmeyer D, Allen PM, Boehm T (2000) Genetically separable determinants of hair keratin gene expression. *Dev Dyn* 218: 537–543

Schüddekopf K, Schorpp M, Boehm T (1996) The whn transcription factor encoded by the nude locus contains an evolutionarily conserved and functionally indispensable activation domain. *Proc Natl Acad Sci USA* 93: 9661–9664

Segre JA, Nemhauser JL, Taylor BA, Nadeau JH, Lander ES (1995) Positional cloning of the nude locus: genetic, physical, and transcription maps of the region and mutations in the mouse and rat. *Genomics* 28: 549–559

Sobhian B, Laguette N, Yatim A, Nakamura M, Levy Y, Kiernan R, Benkirane M (2010) HIV-1 Tat assembles a multifunctional transcription elongation complex and stably associates with the 7SK snRNP. *Mol Cell* 38: 439–451

Strodicke M, Karberg S, Korge G (2000) Domina (Dom), a new *Drosophila* member of the FKH/WH gene family, affects morphogenesis and is a suppressor of position-effect variegation. *Mech Dev* 96: 67–78

Su DM, Navarre S, Oh WJ, Condie BG, Manley NR (2003) A domain of Foxn1 required for crosstalk-dependent thymic epithelial cell differentiation. *Nat Immunol* 4: 1128–1135

Sugimura I, Adachi-Yamada T, Nishi Y, Nishida Y (2000) A *Drosophila* Winged-helix nude (Whn)-like transcription factor with essential functions throughout development. *Dev Growth Differ* 42: 237–248

Sutherland DJ, Li M, Liu XQ, Stefancsik R, Raftery LA (2003) Stepwise formation of a SMAD activity gradient during dorsal-ventral patterning of the *Drosophila* embryo. *Development* 130: 5705–5716

Swann JB, Weyn A, Nagakubo D, Bleul CC, Toyoda A, Happe C, Netuschil N, Hess I, Haas-Assenbaum A, Taniguchi Y et al (2014) Conversion of the thymus into a bipotent lymphoid organ by replacement of FOXN1 with its paralog, FOXN4. *Cell Rep* 8: 1184–1197

Tang AH, Neufeld TP, Rubin GM, Muller HA (2001) Transcriptional regulation of cytoskeletal functions and segmentation by a novel maternal pair-rule gene, lilliputian. *Development* 128: 801–813

Tilney LG, DeRosier DJ (2005) How to make a curved *Drosophila* bristle using straight actin bundles. *Proc Natl Acad Sci USA* 102: 18785–18792

Urano A, Endoh M, Wada T, Morikawa Y, Itoh M, Kataoka Y, Taki T, Akazawa H, Nakajima H, Komuro I et al (2005) Infertility with defective spermiogenesis in mice lacking AF5q31, the target of chromosomal translocation in human infant leukemia. *Mol Cell Biol* 25: 6834–6845

Vaidya HJ, Briones Leon A, Blackburn CC (2016) FOXN1 in thymus organogenesis and development. *Eur J Immunol* 46: 1826–1837

Weiner L, Fu W, Chirico WJ, Brissette JL (2014) Skin as a living coloring book: how epithelial cells create patterns of pigmentation. *Pigment Cell Melanoma Res* 27: 1014–1031

Weiner L, Han R, Scicchitano BM, Li J, Hasegawa K, Grossi M, Lee D, Brissette JL (2007) Dedicated epithelial recipient cells determine pigmentation patterns. *Cell* 130: 932–942

Winter H, Rogers MA, Langbein L, Stevens HP, Leigh IM, Labreze C, Roul S, Taieb A, Krieg T, Schweizer J (1997) Mutations in the hair cortex keratin hHb6 cause the inherited hair disease monilethrix. *Nat Genet* 16: 372–374

Wittwer F, van der Straten A, Keleman K, Dickson BJ, Hafen E (2001) Lilliputian: an AF4/FMR2-related protein that controls cell identity and cell growth. *Development* 128: 791–800

Xu R, Deng K, Zhu Y, Wu Y, Ren J, Wan M, Zhao S, Wu X, Han M, Zhuang Y et al (2008) A large-scale functional approach to uncover human genes and pathways in *Drosophila*. *Cell Res* 18: 1114–1127

Yokoyama A (2018) RNA polymerase II-dependent transcription initiated by selectivity factor 1: a central mechanism used by MLL fusion proteins in leukemic transformation. *Front Genet* 9: 722

Yokoyama A, Lin M, Naresh A, Kitabayashi I, Cleary ML (2010) A higher-order complex containing AF4 and ENL family proteins with P-TEFb facilitates oncogenic and physiologic MLL-dependent transcription. *Cancer Cell* 17: 198–212

Zhu X, Ahmad SM, Aboukhalil A, Busser BW, Kim Y, Tansey TR, Haimovich A, Jeffries N, Bulyk ML, Michelson AM (2012) Differential regulation of mesodermal gene expression by *Drosophila* cell type-specific Forkhead transcription factors. *Development* 139: 1457–1466

Zook EC, Krishack PA, Zhang S, Zeleznik-Le NJ, Firulli AB, Witte PL, Le PT (2011) Overexpression of Foxn1 attenuates age-associated thymic involution and prevents the expansion of peripheral CD4 memory T cells. *Blood* 118: 5723–5731

Zuklys S, Handel A, Zhanybekova S, Govani F, Keller M, Maio S, Mayer CE, Teh HY, Hafen K, Gallone G et al (2016) Foxn1 regulates key target genes essential for T cell development in postnatal thymic epithelial cells. *Nat Immunol* 17: 1206–1215